Coordinated assembly and release of adhesions builds apical junctional belts during *de novo* polarisation of an epithelial tube

Andrew C Symonds[*2], Clare E Buckley[*1,2, 3], Charlotte A Williams[2] & Jonathan DW Clarke[1,2]

* Equal contribution

1. Corresponding authors

2. Centre for Developmental Neurobiology,
Institute of Psychiatry, Psychology and Neuroscience
King's College London
Guy's Campus
London
SE1 1UL

3. Department of Physiology, Development and Neuroscience
University of Cambridge
Downing Street
Cambridge
CB2 3BY

Abstract

Using the zebrafish neural tube as a model, we uncover the *in vivo* mechanisms allowing the generation of two opposing apical epithelial surfaces within the centre of an initially unpolarised, solid organ. We show that NOK/Pals1/Mpp5a and Rab11a play a dual role in coordinating the generation of ipsilateral junctional belts whilst simultaneously releasing contralateral adhesions across the centre of the tissue. We show that Nok and Rab11a mediated resolution of cell-cell adhesions are both necessary for midline lumen opening and contribute to later maintenance of epithelial organisation. We propose these roles for both Nok and Rab11a operate through the transmembrane protein Crumbs. In light of a recent conflicting publication, we also clarify that the junction remodelling role of Nok is not specific to dividing cells.

Introduction

Epithelia are one of the fundamental tissue types of the body, forming protective sheets of cells around the outside of the organism and lining the inside surface of many organs or parts of organs. All epithelia are polarised and have an apical and a basal surface that are molecularly and functionally distinct. In some cases, the organisation of the apical surface of an epithelium is generated at the free surface of an embryonic sheet of cells while in others the apical surface emerges from within a dense rod or ball of cells to generate an epithelial tube or cyst (Martin-Belmonte et al., 2008, Datta et al., 2011). Generating an apical surface from within a rod or ball of cells adds an extra layer of complexity to this process as cells at the centre of these structures have to lose inappropriate connections to generate a free surface. They must also organise that free surface into a typical apical structure comprising a lattice of closely adherent cells connected by apicolateral belts of specialised junctions (typically adherens junctions and tight junctions in vertebrates). A key step, elucidated in epithelial development in flies, is the Crumbs-dependent redeployment of junctional proteins such as Baz (*Drosophila* Pard3) and E-Cadherin from the apical-most surface of single sheet epithelial cells to the apico-lateral border of the cell (Grawe et al., 1996, Harris & Peifer, 2005, McGill et al., 2009, Morais-de-Sa et al., 2010, Pilot et al., 2006, Tepass, 1996). This builds the apicolateral junctional belts that tie the epithelial cells together (St Johnston & Ahringer, 2010, Wei et al., 2005). To what extent similar mechanisms of apical surface development are employed at a free surface compared to within a rod or sphere primordium, and how these can be coordinated with the remodelling of cell-cell connections necessary for *de novo* surface generation, is poorly understood, especially in vertebrates *in vivo*.

Here we analyse the spatial deployment of the cardinal polarity protein Partitioning-defective 3 (Pard3) and the cell adhesion protein N-cadherin (Cdh2) during generation of the apical surface of the neural tube in the zebrafish embryo *in vivo*. Here, the apical surface is generated *de novo* from within the solid neural rod. The relative accessibility and transparency of zebrafish embryos provides an advantageous system in which to address mechanism in whole embryos. We use experimental manipulations of the NOK/Pals1/Mpp5a scaffold protein and the endocytic recycling protein Rab11a. We determine the cellular and molecular mechanisms that release cell adhesions across the organ midline whilst simultaneously generating the canonical apical junctional belt organisation of epithelia within a solid primordium. We compare these to previously shown mechanisms that generate apical organisation at a free surface. We show that both Mpp5a and Rab11a are required to remodel connections between contralateral and ipsilateral cells and suggest they operate through apical recruitment of the transmembrane protein Crumbs.

Results

Apical rings of Pard3 and ZO-1 are built up from the ventral floor plate

The apical surface of epithelia is characterised by a lattice-like arrangement of polarity and scaffolding proteins (such as Pard3, atypical protein kinase C (aPKC), Zonula occludens-1 (ZO-1)) and cell adhesion proteins (such as Cdh2). We visualised this organisation prior to lumen opening in the sagittal plane of the zebrafish neural rod (stages 10 to 18 somites, 14 to 18 hours post fertilization, hpf) at the level of the nascent anterior spinal cord (Figure 1A, B). We generated a BAC transgenic fish line that reports endogenous spatiotemporal expression of Pard3, a cardinal polarity protein, in live embryos (TgBAC(pard3:Pard3-EGFP)^{kg301}, referred to as 'Pard3-EGFP'.

At early rod stages (11 somites), apical rings of Pard3-EGFP and ZO-1 were first established at the midline in ventral floor plate cells (Figure 1B). In more dorsal areas of neuroepithelium, where apical rings had not yet formed, Pard3-EGFP and ZO-1 were seen as puncta (Figure 1B, e.g. arrowheads), reminiscent of spot adherens junctions in other systems (e.g. Tepass et al., 1996). Over the next few hours of rod stage (up to 17 somite stage) the lattice work of apical rings progressively builds from ventral to dorsal such that at any timepoint there is a developmental gradient along the dorso-ventral axis (Figure 1B, E). In contrast to a previous study (Guo et al., 2018) our results suggest that Pard3 is an early component of the nascent apical junction organisation, with both Pard3 and ZO-1 expressed in a punctate manner during a dynamic phase of cell interdigitation across the neural midline (current results and Buckley et al., 2013).

Pard3 puncta initially appear at cell vertices

To understand where in the cell Pard3 puncta first appear, we labelled Pard3-EGFP embryos with membrane-tagged mNeptune2.5 and imaged prior to apical surface formation. Pard3-EGFP puncta were seen close to the midline around the perimeter of cells, often at cell vertices (Figure 1C). Membrane tagged mNeptune was not enriched at vertices, indicating Pard3-EGFP enrichment is not simply due to more membrane at these points. Later, Pard3-EGFP puncta were localised progressively closer together and not confined to cell vertices (Figure 1D). This suggests apical rings may be built by adding Pard3 puncta at cell-cell interfaces until they coalesce to form a more or less continuous ring structure.

nok^{m227} mutants fail to undergo puncta to apical ring transition

To uncover mechanisms that regulate formation of apical junctions in the neural rod we examined apical puncta to ring transition in a mutant fish line that fails to open a lumen.

Nok/Mpp5a is a MAGUK scaffolding protein (Wei & Malicki, 2002), essential to retain all forms of the transmembrane protein Crumbs at the apical surface (Zou et al., 2013). *nok* mutants fail to generate an open a lumen in the neural rod and have disorganised adherens junctions (Lowery et al., 2009, Lowery & Sive, 2005). Although *nok*^{m227} mutants generated Pard3-EGFP puncta in the sagittal plane at the 16 somite stage, these puncta failed to undergo the puncta-to-apical ring transition and remained as punctate deposits (Figure 1H). Nok/Mpp5a is thus critical to build apical junctional rings.

Apical rings on either side of the tissue midline develop independently and are offset from one another

To successfully undergo *de novo* lumen formation, the zebrafish must generate not one, but two lattice-like apical surfaces in the middle of a solid tissue, one on the left side and one on the right side of the future lumen. One possibility is a single plane of apical rings may first develop at the left-right interface and then these pioneer rings split into left and right rings. To assess this, we analysed development of left and right rings. Imaging sagittal and parasagittal planes we never saw an embryo containing a single plane of apical rings (Figure 1F, G, supplementary movie 1). Instead, rings were always found bilaterally, and incomplete apical rings were also found bilaterally on either side of the midline, showing left and right rings are built independently. Furthermore, the developing rings on either side of the midline are always offset from one another, rather than having a mirror-symmetric arrangement that might be expected if individual rings split into two (Figure 1G).

Non-sister connections impose cell offsets across the midline

Most neural rod cells derive from progenitor divisions that generate mirror-symmetrically polarised sisters connected to each other across the midline (the C-division, Buckley et al., 2013, Kimmel et al., 1994, Tawk et al., 2007). This process will at least temporarily align pairs of sister cells across the midline. However, the offset organisation of left and right apical rings later in development suggests a mechanism exists that adds offset to this initial alignment. To confirm that sister cells become offset, we generated mosaically labelled embryos and used live imaging to assess the interface between sister cells. Soon after a C-division, sister cells appeared mirror-symmetric to each other across the tissue midline (Figure 2A, 13 somites). However, the shape of nascent apical endfeet changed over time, likely in response to movements and mitoses of neighbouring (unlabelled) cells (Figure 2A and supplementary movies 2-4). The location of the sister-cell interface in relation to the rest of the cell shape therefore also changed until the neural rod stage, when the connection between the sisters was stably offset such that nascent apical endfeet of sister cells met at their corners (Figure 2A, 18 somites). Thus, an initially mirror-symmetric sister cell alignment is shifted to an offset

organisation following C-division mitosis. The offset conformation suggests that contralateral cell connections across the midline are likely not confined to their C-division sisters.

To examine the dynamics of ipsilateral and contralateral cell adhesions during the process of the midline C-division, we used a BAC transgenic line expressing the cell adhesion protein Cdh2 fused to a tandem fluorescent timer (Revenu et al., 2014). Cdh2-GFP is expressed in neural rod cells over the entire plasma membrane. Prior to C-divisions, cells intercalated across the midline and Cdh2-GFP was enriched in this interdigitation zone, showing that cells contact and adhere to several contralateral, as well as ipsilateral, cells (Figure 2Bi). When cells entered C-division mitosis near the midline, cell processes from neighbouring cells ingressed into the cleavage furrow and distinct enrichments of Cdh2-GFP became largely localised to the cleavage furrow during telophase (red arrows, Figure 2Bi). This cell ingression allowed neighbouring cells to contact and presumably adhere to both ipsilateral and contralateral daughters of the C-division. Cell ingression into the cleavage furrow therefore provides a potential mechanism to promote connections between multiple contralateral and ipsilateral cells (as cartooned in figure 2Biii).

By the 17 somite stage, Cdh2-GFP was enriched at the interface between left and right cells, sometimes at the apical cell vertices (Figure 2Bii). By this stage the left-right interface was largely a straight line at the midline. To see whether the offset cell conformation between cells on the left and right persists until lumen opening, we examined electron micrographs taken at the start of lumen inflation. This showed a striking zig-zag conformation between cells separating across the midline (Figure 2C). It appears the offset conformation between left and right cells persists until the lumen inflates, separating the left and right sides of neural rod.

In summary, this data suggests the C-division can promote connections between multiple ipsilateral and contralateral cells during epithelialisation. We suggest the maintenance of these connections until rod stage would promote an offset conformation between sister cells.

A single midline interface enriched in polarity and cell adhesion proteins precedes bilateral apical rings

To understand the transition from spot-like junctional specialisations to two independent lattices of apical rings on left and right sides of the midline we analysed the distribution of Pard3 and Cdh2 during this transition. Since there is a developmental gradient along the dorso-ventral axis of the neuroepithelium (Figure 1B and E), we focused on a mid-dorsoventral plane of the anterior spinal cord. We imaged Pard3-EGFP and Cdh2-GFP from neural keel to neural rod stages in the horizontal plane (Figure 3Ai-iii). Pard3-EGFP and Cdh2-GFP initially had different

patterns of expression. At 11 somites (14 hpf) puncta of Pard3-EGFP were localised broadly around the midline, along interfaces between interdigitating cells. These correspond to the spot distribution of Pard3-EGFP seen sagittally (Figure 1B and C). At the same timepoint Cdh2-GFP was expressed at low levels throughout the cell membrane but also slightly elevated in the interdigitation zone, mostly in discrete spots. By 17 somites (17.5 hpf), both Cdh2-GFP and Pard3-EGFP were clearly enriched at the neural rod midline in a near continuous, fairly straight expression domain at the interface between left and right cells. Consistent with a developmental gradient along the dorso-ventral axis of the neuroepithelium, dorsal to this plane, Pard3-EGFP was still expressed in a discontinuous mediolateral stripe pattern, and ventral to this it appeared in two parasagittal domains either side of the midline (Figure 3Av). The intermediate level that shows a single left-right interface of Pard3-EGFP expression occupies a small and transient dorsoventral domain that moves dorsally as the assembly of bilateral rings progresses ventral to dorsal.

To analyse the distribution of cell membranes relative to the expression of Pard3-EGFP, we revealed membranes by injecting embryos with mRNA mNeptune2.5-CAAX. By 24 hpf, although spinal cells at almost all dorsoventral levels did still meet at the left-right interface (see Figure 3vi), Pard3-EGFP and Cdh2-GFP no longer localised to this interface; rather their expression had transitioned from mediolaterally arranged puncta through a single midline domain and into two parasagittal domains either side of the midline (Figure 3Ai, iv). These two domains were characterised by periodically elevated spots of expression that correspond to points within the left and right apical rings. Much lower levels of Pard3-EGFP and Cdh2-GFP remained in the medial zone between bilateral apical rings (Figure 3Ai, iv).

Nok/Mpp5a is required to redeploy adhesions to the apicolateral border

Although eliminating Crumbs in zebrafish is difficult because there are multiple Crumbs proteins, we took advantage of the *nok*^{m227} mutant that is unable to localise Crumbs proteins to the apical surface (Zou et al., 2013). Since we demonstrated that the apical spot to ring transition did not occur in *nok*^{m227} mutants (Figure 1H), we wanted to test the role for Nok in displacing Pard3 and Cdh2 proteins from a single line at the left-right interface, to the bilateral expression domains seen at later time points. For this we generated a *nok*^{m227} mutant; Cdh2-tFT compound transgenic line. Whereas 'wild-type' Cdh2-tFT embryos opened a lumen in hindbrain and anterior spinal cord (Figure 3Bi), *nok*^{m227}; Cdh2-tFT embryos failed to open a lumen (Figure 3Bii), in line with previous observations of *nok* mutant embryos (Lowery & Sive, 2005).

To understand the *nok*^{m227} phenotype in relation to Cdh2 remodelling and its relation to Crumbs expression, we examined their localisation in wild-type and *nok*^{m227} embryos. In wild-type

embryos (Figure 3Ci) Crumbs2a was first expressed at the neural rod 17/18 somite stage at the left-right interface, coincident with a single line of expression of Cdh2. However, by 26 somites, when Crumbs2a was still localised to the left-right interface, Cdh2-GFP protein was displaced to form two slightly more basolateral lines of expression. Cdh2-GFP expression was located immediately lateral to Crumbs2a, with little overlap of expression.

In *nok*^{m227} mutant embryos (Figure 3Cii) Crumbs2a was absent from the midline as expected. At the 18 somite stage *nok*^{m227} mutant Cdh2-tFT embryos showed a single domain of enrichment of Cdh2-GFP at the left-right interface similar to wild-type Cdh2-GFP embryos. However, unlike wild-type embryos, Cdh2-GFP remained as a single midline domain in *nok*^{m227} mutants failing to undergo the transition to two lines of Cdh2-GFP either side of the midline, even up to stages as late as 28 hpf.

Together, these data show left and right cells initially adhere together across the midline through contralateral adhesions. However, both Cdh2 and Pard3 are then redeployed more basally to the apicolateral border where they contribute to adhesive junctions between ipsilateral cells to build coherent, bilateral sheets of neuroepithelium. This redeployment of junctional proteins depends on Nok/Mpp5a and is likely to be a critical step in releasing cells from their contralateral adhesions to allow lumen formation.

Persistent adhesions may contribute to lack of epithelial maintenance in Nok and Rab11a deficient epithelia

To test whether Nok deficient cells retain persistent adhesions across the midline, we analysed the behaviour of clonally related cells in the hindbrain regions of 25 hpf wild-type embryos that had open lumens and *nok* morphant embryos that were unable to open a lumen. In wild type embryos, cells successfully separated across the midline following C-division; they maintained an elongated morphology that stretched from the apical to basal surface and later differentiative divisions (D-divisions) occurred at the apical surface (Figure 4A). However, in *nok* morphant tissue, cells were not separated across the midline, often did not fully extend to the basal surface and they appeared clumped together, often in rosette-like structures. D-divisions in *nok* morphants occurred within these cell clumps, often at a distance from the midline of the tissue, (Figure 4B and 4C). The behaviour of ectopic divisions in *nok* morphants is accompanied by a lateral dispersal of Pard3 from the midline (Figure 4D). Thus, as well as being unable to undergo the puncta to apical ring transition (Figure 1H), Nok deficient cells show persistent adhesions and apical midline organisation becomes progressively fragmented over time.

Since we hypothesise that Nok functions through its ability to localise Crumbs to the nascent apical surface, we next analysed cell behaviours following another manipulation that depletes Crumbs from the apical surface. We expressed a dominant-negative (DN) form of Rab11a in rhombomeres 3 and 5. We previously showed this manipulation reduces apical Crumbs 2a localisation and prevents lumen opening in these segments (Buckley et al., 2013). Here, we show that apical Crumbs 1 is also downregulated in DNRab11a rhombomeres (Figure 4E), confirming this manipulation is sufficient to downregulate apical trafficking of multiple Crumbs paralogs. Cells in DNRab11a rhombomeres did not separate following D-division and formed cell clumps and rosette-like structures with a central focus of Pard3 (Figure 4F,G). Similar to *nok* morphants (Figure 4D), a lateral dispersal of Pard3-EGFP from the midline was seen, progressively fragmenting midline organisation over time (Figure 4H). This supports our previous observations of ZO-1 dispersion in DNRab11a segments (Buckley et al., 2013). Staining of DNRab11a rhombomeres revealed ectopic clumps of Pard3 and centrosomes, sometimes arranged in rosette-like structures with centrally located Pard3 surrounded by centrosomes (Figure 4I and J).

Interestingly, whilst cells situated in the middle of closed-lumen DNRab11a rhombomeres 3 and 5 formed clumps, cells at the edges of these rhombomeres often had a typical elongated neuroepithelial morphology. These were able to build an aPKC positive apical surface that was contiguous with the wild-type apical surface in adjacent open-lumen wild-type rhombomeres 2, 4 and 6 (Figure 5A). Edge cells were oriented obliquely along the anterior-posterior axis of the embryo, apical towards the open lumens (e.g. arrows in figure 5Aii). To determine how this morphology arose, we made time-lapse movies of DNRab11a/wild-type interface neuroepithelial cells. We found interface cells remained connected across the midline as the neighbouring wild-type lumen inflated, acting like a hinge and reorienting cells at the DNRab11a/wild-type rhombomere boundary towards the opening lumen (Figure 5Bi). Despite persistent connections between cells, the DNRab11a luminal surface expanded via cell division and subsequent reintegration into the epithelium (Figure 5Bii). Cell divisions in the centre of DNRab11a rhombomeres were disorganised and did not orient along the tissue midline, whilst those occurring at the DNRab11a luminal surface occurred with parallel orientation (Figure 5Biii.) These results demonstrate that DNRab11a cells at the DNRab11a/wild-type interface are able to successfully reintegrate into the epithelium following division if they have access to an apical lumen surface.

Our data suggests that persistent adhesions between cells in Nok deficient and DNRab11a

embryos both inhibits lumen formation and promotes the formation of local clumps of cells. This results in the progressive fragmentation of midline organisation over successive rounds of division in Nok deficient and DNRab11a embryos.

Nok is necessary for apical ring formation even in the absence of cell division.

To address whether Nok function may be specifically related to resolving connections between sister cells (as suggested in Guo et al. 2018), we analysed the key events of apical ring formation in *nok*^{m227} mutant embryos with and without C-divisions. Since the closed-lumen phenotype is not fully penetrant in some regions of the *nok* mutants (Supplementary Figure 2), we suggest that using apical ring formation rather than lumen opening is a better test of function. We blocked C-divisions using the S-phase inhibitor Aphidicolin and analysed Pard3-EGFP in the anterior spinal cord region. Apical rings of Pard3-EGFP are not rescued by blocking C-divisions in *nok*^{m227} mutants (Figure 6). The efficacy of the division block was confirmed by the enlarged nuclear size in aphidicolin treated embryos (Figure 6F and G) and the fewer, enlarged apical rings in the aphidicolin treated siblings (Figure 6B and H). These results demonstrate that, whilst necessary for cell-cell separation following division, Nok function is not specifically related to remodelling adhesions between C-division sisters. Instead it plays a more fundamental role in the formation of apical junctional rings and release of contralateral adhesions during *de novo* polarisation of an epithelial tube.

Discussion

The development and remodelling of apical epithelial junctions is likely to be regulated by a complex integration of molecular interactions involving polarity proteins and adhesion proteins (Martin-Belmonte et al., 2008, St Johnston & Ahringer, 2010, Datta et al., 2011), together with biomechanical forces that interpret tissue tensions generated by the actomyosin cytoskeleton (Pinheiro and Bellaiche, 2018). Here we have investigated some of the cellular and molecular features that underlie *de novo* apical surface generation within the solid rod primordium of the embryonic zebrafish central nervous system. Our work uncovers three aspects of *de novo* apical surface generation within a complex organ *in vivo*. First, despite the very different cellular organisations, apical surface generation at the centre of a solid organ primordium follows a strikingly similar sequence of spot to ring junction building to those previously described for apical surface generation at a free surface of a sheet of cells. Second the displacement of

proteins from the nascent apical surface to the nascent apicolateral junctional belt domain serves two purposes in a solid organ primordium; it simultaneously contributes to the building of epithelial junctional belts and releases adhesions with contralateral cells that would otherwise inhibit the generation of a free surface and lumen formation. Thirdly neuroepithelial cell divisions across the nascent apical plane (C-divisions) do not promote exclusive connections between contralateral sister cells. Instead connections between multiple ipsilateral and contralateral partners are promoted by neighbour ingression into the cleavage furrow of the C-division and appear to contribute to the offset alignment of contralateral cells across the midline. Through this realignment, sister cells do not remain connected '*en face*' as previously suggested (Guo et al., 2018), but instead sisters become attached in an offset configuration from one another across the midline. In addition, we address a recent suggestion that the MAGUK scaffolding protein Nok is only required to remodel apical protein location following cell divisions across the nascent apical plane (Guo et al., 2018). We show this is not the case as Nok-dependent apical protein remodelling is required for apical surface generation both with and without cell divisions.

Roles of Nok and Rab11a

We describe a similar displacement of Pard3 and Cdh2 to the apicolateral cell of zebrafish neuroepithelial cells as that seen in *Drosophila* ectodermal cells (Grawe et al., 1996, Harris & Peifer, 2005, McGill et al., 2009, Morais-de-Sa et al., 2010, Pilot et al., 2006, Tepass, 1996). In the zebrafish neural rod the displacement occurs at the midline within a solid rod of cells rather than at a free surface, but despite this fundamental difference in tissue architecture, a similar mechanism appears to build the apicolateral junctional belts. We show that the scaffold protein Nok/Mpp5 is necessary for the displacement of Pard3 and Cdh2 and for the formation of apical rings. In line with the *Drosophila* literature mentioned above, we propose Nok operates through its role in scaffolding Crumbs to the apical surface. This is consistent with the appearance of Crumbs at the nascent apical surface when Pard3 and Cdh2 are displaced from this surface and the lack of Crumbs localisation to the nascent apical surface in *nok* mutants (Figure 3C and Zou *et al.* 2013). A direct test of Crumbs function is difficult in zebrafish because three different Crumbs proteins (Crb1, Crb2a and Crb2b) are present at this stage in the developing neural rod. Previous research has shown that neuroepithelial organisation was only altered when all paralogs of Crumbs protein were knocked down by multiple morpholinos (Zou *et al.* 2013) and, consistent with our hypothesis, this appears to include a lack of lumen formation. Rather than transiently knocking down all paralogs of Crumbs proteins in this study, we used a Nok mutation (*nok*^{m227}) that downregulates all paralogs of Crumbs protein from the nascent apical surface. In this case neither Pard3 nor Cdh2 were displaced from the nascent apical surface and this resulted in persistent adhesions between left and right sides of the neural rod and a loss of lumen formation. Additionally, we found that a stable genetic manipulation of Rab11a which also

lacks Crumbs at the nascent apical surface (Roeth *et al.* 2009, Buckley et al 2013) also showed persistent adhesions between contralateral cells, a lack of lumen opening and, at later stages, comparable disorganisation of neuroepithelial tissue to *nok* mutants (Figure 4).

Despite its function in mediating epithelial cohesion via homophilic interactions of its extracellular domain (Thompson et al., 2013), the role of Crumbs protein in allowing cells to resolve their apical adhesions is emerging as another important mechanism for controlling epithelial morphogenesis. For example, a recent study demonstrated a secreted version of Crumbs2 acted non-cell autonomously to cause delamination of neuroepithelial cells during dorsal collapse of the spinal cord central canal in mouse embryos (Tait et al., 2020). By studying dominant-negative Rab11a cells in an environment where they have access to wildtype neighbours, we uncovered that cells depleted of Crumbs from their apical surface can none-the-less form an epithelial surface when adjacent to wildtype cells. Thus, in the fish neuroepithelium, Rab11a and Crumbs appear to be required for *de novo* epithelial surface generation but dispensable for integration next to an already generated apical surface. This suggests that non cell-autonomous rescue from neighbouring wildtype cells is able to initiate epithelialisation in the absence of Rab11a/Crumbs. It would be interesting to determine whether secreted Crumbs protein plays a role in this rescue.

Coordinating left-right release with epithelialisation

The zebrafish neural rod is initially a solid primordium, so the displacement of Pard3 and Cdh2 is not from a free apical surface but instead occurs within the densely packed cell-cell interfaces that lie at the tissue centre. Cell adhesions between contralateral cells across the neural rod initially bind left and right halves of the neural rod together, but these adhesions need to be released to generate the lumen and apical surface of the neuroepithelium. We show Nok neatly coordinates the release of contralateral connections with the strengthening of ipsilateral connections, thus leading both to the generation of a free surface within the centre of an initially solid tissue and to junctional belt formation and epithelialisation. Nok-deficient cells were unable to form a coherent sheet of apical rings (figure 1H). Additionally, in the absence of Nok or the presence of DNRab11a cells were unable to release cell-cell adhesions. During epithelialisation, these defects first resulted in closed lumens (Figure 3B and 4Hi). This is in line with our previous findings (Buckley et al., 2013) and others' findings that apical localisation of Rab11 is necessary for cell abscission and normal opening of Kupffer's vesicle in zebrafish (Rathbun et al., 2020). It would be interesting to know whether similar mechanisms also operate in the caudal segments of avian and mammalian spinal cord. The neural tube in these segments forms through the process of secondary neurulation that also involves the *de novo* formation of

a central lumen within a condensing rod of cells (see Schoenwolf 1984, Dady et al 2014), rather than epithelial folding that generates the neural tube in more rostral segments of these animals.

At later stages of development in the zebrafish neural tube, when neuroepithelial cells undergo interkinetic nuclear migration and D-divisions, the absence of Nok or the presence of DNRab11a resulted in progressive disintegration of midline organisation (Figure 4D and H). This may be due to a combination of factors; during cell division, interkinetic nuclear migration and mitotic rounding pull cells around within the tissue. In a normal epithelium the apical surface would be stabilised by the lattice of ring-like junctional belts that hold the apical surface together. But when junctional belts between ipsilateral cells are not present, the tissue fails to hold cells at the apical plane and cells are unable to fully re-extend to the basal side of the neural rod following division. Additionally, a lack of cell separation following division promotes the formation of local clumps of cells. Together, these defects cause divisions to occur in ectopic locations and the midline organisation disintegrates.

Our results suggest an abnormal persistence of cell adhesions is a key part of the *nok* and DNRab11a phenotypes and suggests a lack of cell-cell separation may contribute to other epithelial disorganisation phenotypes in Crumbs or Rab11a-deficient epithelia (Das & Knust, 2018, Roeth et al., 2009).

Role of the C-division

A recent paper also concluded that Nok is necessary to remodel junctional proteins during epithelialisation in the neural rod (Guo et al., 2018). They however propose Nok's role in apical remodelling is only necessary to rescue potential tissue disruption caused by midline C-divisions, a conclusion based on their reported rescue of lumen formation and apical junctional belts when cell division is blocked in the *nok*^{m520} mutant (discussed in Supplementary Data). However, we show that blocking cell division does not rescue junctional belt formation in *nok*^{m227} mutants (Figure 6), and has a more fundamental role in apical junction remodelling than resolving cell connections during C-divisions.

We previously demonstrated that C-divisions at the neural rod midline are an important morphogenetic force during neural tube formation. Ectopic divisions are able to organise ectopic neural lumens and duplicate the neural tube (Tawk et al., 2007) while neural tubes generated in the absence of C-divisions are less efficient at resolving cell interdigitation across the midline and have a disorganised morphology (Buckley et al., 2013). Here we show connections between ipsilateral and contralateral cells are pulled into the cleavage furrow of C-divisions (Figure 2). This ingression of neighbours into the cleavage furrow is reminiscent of neighbour

ingression during mitoses in *Drosophila* epithelia (Herszterg et al., 2013). Invasion of neighbours into the cleavage furrow also occurs during chick gastrulation where it can be developmentally regulated to promote or impede cell intercalation between daughter cells and hence contribute to control of morphogenetic movements (Firmino et al., 2016). In zebrafish, we show multiple contralateral cell contacts are promoted through ingression of neighbouring cell processes into the cleavage furrow. We propose the maintenance of connections with multiple contralateral cells through C-divisions ensures cells do not solely connect to their sisters and suggest this is one mechanism that leads to staggered connections across the midline. This staggered alignment of endfeet may generate a morphogenetic advantage by allowing attachment to a larger number of cells than a one-to-one 'mirror adhesion' and therefore helps colocalise apical junctions from multiple neighbouring cells to the midline. The localisation of junctional proteins at cell corners might also be important for allowing flexibility of cell movement during tissue remodelling (Finegan et al., 2019).

It is also likely that actinomyosin generated forces at the neural rod midline will contribute to apical junction assembly. Both actin (Yang et al., 2009) and non-muscle myosin (Gutzman and Sive, 2010) accumulate at the developing apical plane and there is substantial evidence that biomechanical forces play a role in adherens junction dynamics in other systems (Pinheiro and Bellaiche, 2018). Recent findings also show actomyosin mediated tension is necessary for assembling ZO1 at tight junctions during zebrafish gastrulation (Schwayer et al., 2019). So, in addition to the role of microtubules (Buckley et al 2013), it would be interesting to see what role actomyosin mechanics play in the assembly of apical junctions within the zebrafish neural rod.

Methods

Embryo Care

All embryos were collected, staged and cultured according to standard protocols (Kimmel et al., 1995). All procedures were carried out with UK Home Office approval and were subject to local Ethical Committee review.

Generation of Pard3-EGFP transgenic line

To generate the transgenic zebrafish line expressing Pard3-EGFP with endogenous spatial and temporal expression we used bacterial artificial chromosome (BAC) recombineering. We replaced the stop codon of the pard3-003/ASIP transcript (von Trotha et al., 2006), in the BAC clone DKEY-71E21 (Source Bioscience). This BAC clone contains ~71 kb upstream of the pard3-003/ASIP start codon and ~30 kb downstream from the targeted stop codon. We followed

the protocol of (Bussmann & Schulte-Merker, 2011), with some modifications. The original protocol leaves a kanamycin selection cassette in the final BAC construct. However, we found this led to cell death and a lack of endogenous Pard3-EGFP expression. To remove the kanamycin selection cassette, we substituted two reagents with those from the Sarov *et al.,* 2006 recombineering protocol and added an extra 'flip out' step to remove the kanamycin cassette. Specifically, we used the pRedFlp4 and R6k-EGFP-FRT-kanR-FRT cassettes from Sarov *et al* 2006. The EGFP-FRT-kan-FRT targeting cassette was PCR amplified with 50 bp homology arms at either end, to target it to replace the pard3-003/ASIP stop codon during BAC recombineering.

Forward primer:

5'-

CACAGAAGCAGAACGGACGCAATGGACACCCCTCCACTTCAGACAGGTAC**AGCTCAGGA GGTAGCGG** -3'

and reverse primer:

5' -

AATTGAGTTTCATGATAGAACTTTGTATTTCTGCAATTCTGAAAAGCTGA**GGCAGATCGTCA GTCAG** -3'.

The protocol for pRedFlp4 transformation, targeted recombination steps and removal of the kanamycin resistance selection marker by pRedFlp4 induced flipase were carried out as previously described (Sarov et al., 2006), with slight modifications. Briefly, the recombineering pipeline was modified to have two rounds of tagging by Red/ET recombination, the first was insertion of iTol2_amp into the BAC backbone and the second insertion of EGFP-FRT-kanR-FRT. Successful recombination was assessed by colony PCR and then full sequencing of the sites of recombination. Preparation and injection of BAC DNA and screening for transgenic founders was all performed according to standard protocols (Bussmann & Schulte-Merker, 2011; Suster et al., 2011).

Zebrafish Lines

The TgBAC(pard3:Pard3-EGFP)^{kg301} was generated as detailed above. The TgBAC(cdh2:Cdh2-tFT) (Revenu et al., 2014), was kindly provided by Darren Gilmour. The TgBAC(cdh2:Cdh2-tFT) line expresses both Cdh2-sfGFP and Cdh2-tagRFP, but we only image Cdh2-sfGFP expression in our experiments and refer to this as Cdh2-GFP for simplicity. These lines were bred with the Nok^{m227} mutant fish line (Wei & Malicki, 2002a) to generate compound Nok^{m227}; Cdh2-tFT and Nok^{m227}; Pard3-EGFP fish. To prevent ventricle opening in rhombomeres 3 and 5, we crossed the UAS-inducible dominant-negative Rab11a line, Tg(UAS:mCherry-Rab11a S25N)^{mw35} (Clark et al., 2011), with Tg(Krox20:RFP-KalTA4), which drives the optimised Gal4-activator, KalTA4, only in Krox20 positive rhombomeres 3 and 5 (Distel et al.,

2009). This resulted in the expression of Rab11a-S25N specifically in rhombomeres 3 and 5 as previously described (Buckley et al., 2013).

RNA preparation and injection

Fusion constructs containing cDNA in the pCS2+ vector were linearized and mRNA was synthesised using the SP6 mMessage mMachine kit (Ambion, AM1340). RNA for the following constructs was injected using standard protocols (Westerfield, 2000) at 40-100pg per embryo: Histone 2A tagged with GFP (H2A-GFP), Human Histone 2B tagged with RFP (H2B-RFP), Human CAAX membrane moiety tagged with EGFP, mCherry or mNeptune2.5 (EGFP-CAAX, mCherry-CAAX, mNeptune2.5-CAAX), Dominant-negative Human rab protein 11a tagged with EGFP (RAB11A-S25N-EGFP), Zebrafish partitioning-defective 3 tagged with GFP or RFP (Pard3-GFP/RFP). For ubiquitous distribution of mRNA, embryos were injected at the 1-2 cell stage. For mosaic labelling a single blastomere of a 16-64 cell stage embryo was injected.

Morpholino injections

Co-injection of *nok* splice blocking morpholinos (donor: 5'- GTT TAT GAC ACC CAC CTA GTA AAG C -3' and acceptor: 5'- CTC CAG CTC TGA AAG TAC AAA CAC A -3'), was made into one-cell stage embryos (Hsu et al., 2006). Full loss of Crb2a from the midline and associated phenotypes were seen with approximately 1.7 nL of 300 mM (0.5 pM) of each morpholino, which closely phenocopied the *nok* mutant phenotype (this manuscript Supplementary Figure 1 and Hsu *et al.* 2006). Mild to intermediate loss of Crb2a from the midline was seen with approximately 0.5-1 nL of 200-300 mM (0.1-0.3 pM) of each morpholino. The level of Crb2a loss correlated with the extent of associated phenotypes (see Supplementary Figure 1). Standard morpholino sequence was 5'-CCT CTT ACC TCA GTT ACA ATT TATA 3'.

Chemical inhibition of cell division

Cell division was blocked by incubating dechorionated embryos in 300 µM aphidicolin (Sigma) in 4% DMSO from bud stage (10 hpf) to 28 somite stage (23 hpf). Control embryos were incubated in 4% DMSO only. Embryos were maintained on a bed of agarose in 12-well plates in the dark throughout the drug incubation.

Immunohistochemistry

Embryos were fixed with 4% paraformaldehyde for 2 hours at room temperature prior to processing for immunohistochemistry. The following primary antibodies were used: mouse anti-Crb2a (mouse monoclonal, ZIRC zs-4, 1:200), rabbit anti-Crb2a and anti-Crb1 (a kind gift from

the Wei lab, 1:350), mouse anti-ZO-1 (mouse monoclonal, Invitrogen 33-9100, 1:500), rabbit anti-aPKC (rabbit polyclonal, Santa Cruz sc-216, 1:300), mouse anti-γ tubulin (mouse monoclonal, MilliporeSigma T6557, 1:200) and mouse anti-ZO-1 (Life Technologies, 1:300). Rabbit anti-Pard3 (rabbit polyclonal, Millipore 07-330, 1:100) was used following fixation in Dent's for 3 hours at room temperature and rehydration from methanol. AlexFluor secondary antibodies (Life Technologies) were used at 1:500 and Hoeshct (Life Technologies) nuclei stain was used at a final concentration of 1:10,000.

Electron microscopy

Embryos were fixed in 2% paraformaldehyde and 1.5% glutaraldehyde in 0.1 M sodium cacodylate buffer over-night and then processed through 1% osmium and stained in 0.5% uranyl acetate. They were then dehydrated in ethanol and processed through propylene oxide into 100% resin, embedded and baked. Ultra-thin sections were taken in transverse orientation and imaged on a transmission electron microscope.

Confocal imaging and processing

Embryos were mounted in low melting point agarose and imaged either using a Zeiss LSM 880 Fast Airyscan microscope and water dipping x20/1.0 N.A. objective, a Leica SP5 confocal microscope and water dipping x25/0.95 N.A objective or a PerkinElmer Ultraview spinning disk microscope. Imaging at the centre of a developing live tissue mass required the improved resolution in x, y and z obtained by using the Fast Airyscan mode of the Zeiss LSM 880 Fast Airyscan microscope. By using this microscope, high-resolution images of both *en face* Pard3-EGFP rings and the spatial location of Crb2a, aPKC and Cdh2-EGFP in the developing embryo were obtained. To further improve lateral imaging, fish were mounted on an agarose bed with small depressions to hold the yolk of the embryo in place. These agarose beds were made using a custom mould (a kind gift from Andrew Oates). Data was collected from the hindbrain and anterior spinal cord regions. Some adjacent cells have been removed from images of single cells to increase clarity of the cells of interest. Images were processed using Imaris, Volocity and Fiji/ImageJ.

Data analysis

The custom R code used to generate plots for figures 1 and 3 is available at https://github.com/andyivanhoe/pard3-analysis.

To obtain apical ring density counts across the developing neuroepithelium (Figure 1E), Pard3-EGFP embryos were live-imaged en face between 15ss and 21ss using the Zeiss Airyscan. The

dorso-ventral axis of the resulting z-stacks were divided into four quadrants (dorsal, mid-dorsal, mid-ventral, ventral), by applying a grid in Fiji. Apical rings were counted when all sides of the cell border had Pard3-EGFP signal along them.

To quantify the changing distribution of Pard3-EGFP across the neural rod midline over time we imaged 6 live TgBAC(pard3:Pard3-EGFP)^{kg301} embryos over a period of 3 hours using Zeiss Airyscan confocal acquisition and processing. We then made a maximum intensity projection of a 10 µm deep volume at a mid-dorsoventral level of the neural rod. A mediolateral line of 116 µm width was then drawn across the basal to basal width of the developing neuroepithelium and the mean fluorescence intensity at each pixel along that line measured using FIJI. This was repeated for 6 embryos at 1 hour intervals (Figure 3Aii, iii. 0 hours is 16 somite stage). All line profiles from different embryos and timepoints were aligned on the maximum intensity value for each line profile. The central 70 µm of the line profiles, centred on the maximum intensity values, were then used to calculate mean intensity and standard deviation at each point along the line for each timepoint before plotting. We aligned on maximum intensity value for each line profile because the exact maximum intensity of Pard3-EGFP relative to the tissue midline has slight biological variation between embryos.

To quantify the distribution of Pard3-EGFP at the midline at the fully neuroepithelial stage (after the single midline peak had resolved into what appeared to be two near parallel lines of expression on either side of the midline), we analysed a single z-level in the same 6 embryos where the two lines of expression were approximately 4 µm apart (Figure 3Aiv). This analysis was done at the last timepoint of the 3-hour timeline, but at a more ventral (and hence more morphogenetically advanced, see Figure 1 and associated text) position. In this case we measured intensity along a 23 µm wide mediolateral line. Because the midline expression is not perfectly straight and the peaks of expression only 4 µm apart, for this analysis we choose a single z-level and a thinner mediolateral line than for the timeline measurements to avoid averaging out the two peaks.

Plots in figure 4C, 4J, 7G and 7H were generated using Graphpad Prism. Specific statistical analyses are described in the figure legends.

Acknowledgements

We thank Rachel Moore, Christopher Rookyard, Vineetha Vijayakumar and Xuan Liang for helpful discussions on this work. We thank Florent Campo-Paysaa for providing some of the movies analysed in figure 4H and 5B. We thank the Centre for ultrastructural imaging at KCL and the Cambridge Advanced Imaging for their help with processing electron microscopy

samples. We thank the zebrafish facility in KCL for their help maintaining zebrafish stocks. We thank Darren Gilmour for the Cdh2:(Cdh2-tFT) line, Gwyn Gould for RAB11A-S25N-EGFP plasmid, Xiangyun Wei for the Crb2a antibody and Stefan Schulte-Merker and Mihail Sarov for BAC plasmid reagents. This work was supported by UK BBSRC grant BB/K000926/1 (JC), a Wellcome Trust Investigator Award (JC) and a Wellcome Trust/ Royal Society Sir Henry Dale Fellowship (CB).

Author contributions

Conceptualization: AS, CB, JC

Investigation: AS, CB, CW, JC

Writing, reviewing & editing: AS, CB, JC

Supervision: CB, JC

Funding acquisition: CB, JC

References

Buckley, C.E., Ren, X., Ward, L.C., Girdler, G.C., Araya, C., Green, M.J., Clark, B.S., Link, B.A. and Clarke J.D.W. (2013). Mirror-symmetric microtubule assembly and cell interactions drive lumen formation in the zebrafish neural rod. *EMBO J.* **32**, 30-44.

Bussmann, J. and Schulte-Merker, S. (2011). Rapid BAC selection for tol2-mediated transgenesis in zebrafish. *Development* **138**, 4327-32.

Clark, B.S., Winter, M., Cohen, A.R. and Link, B.A. (2011). Generation of Rab-based transgenic lines for in vivo studies of endosome biology in zebrafish. *Dev. Dyn*. **240**, 2452-2465.

Dady, A., Havis, E., Escriou, V., Catala, M. and Duband, J.L. (2014). Junctional Neurulation: A unique developmental program shaping a discrete region of the spinal cord highly susceptible to neural tube defects. *Journal of Neuroscience* **34**, 13208–13221.

Das, S. and Knust, E. (2018). A dual role of the extracellular domain *Drosophila* Crumbs for morphogenesis of the embryonic neuroectoderm. *Biol Open* **7**, bio031435.

Datta, A., Bryant, D.M. and Mostov, K.E. (2011). Molecular regulation of lumen morphogenesis. *Curr. Biol.* **21**, R126-136.

Distel, M., Wullimann, M.F. and Koster, R.W. (2009). Optimized Gal4 genetics for permanent gene expression mapping in zebrafish. *Proc Natl Acad Sci U S A* **106**, 13365-13370.

Finegan, T.M., Hervieux, N., Nestor-Bergmann, A., Fletcher, A.G., Blanchard, G.B. and Sanson, B. (2019). The tricellular vertex-specific adhesion molecule Sidekick facilitates polarised cell intercalation during Drosophila axis extension. *PLoS Biol.* **17**, e3000522.

Grawe, F., Wodarz, A., Lee, B., Knust, E. and Skaer, H. (1996). The Drosophila genes crumbs and stardust are involved in the biogenesis of adherens junctions. *Development* **122**, 951-959.

Guo, C., Zou, J., Wen, Y., Fang, W., Stolz, D.B., Sun, M. and Wei, X. (2018). Apical cell-cell adhesions reconcile symmetry and asymmetry in Zebrafish neurulation. *iScience* **3**, 63-85.

Gutzman, J.H and Sive, H. (2010). Epithelial relaxation mediated by the myosin Phosphatase regulator Mypt1 is required for brain ventricle lumen expansion and hindbrain morphogenesis. *Development* **137**, 795-804.

Harris ,T.J. and Peifer, M. (2005). The positioning and segregation of apical cues during epithelial polarity establishment in Drosophila. *J. Cell. Biol.* **170**, 813-823.

Herszterg, S., Leibfried, A., Bosveld, F., Martin, C. and Bellaiche, Y. (2013). Interplay between the dividing cell and its neighbors regulates adherens junction formation during cytokinesis in epithelial tissue. *Dev. Cell* **24**, 256-270.

Hsu, Y.-C., Willoughby, J.J., Christensen, A.K. and Jensen, A.M. (2006). Mosaic Eyes is a novel component of the Crumbs complex and negatively regulates photoreceptor apical size. *Development* **133**, 4849-4859.

Kimmel, C.B., Ballard, W.W., Kimmel, S.R., Ullmann, B. and Schilling, T.F. (1995). Stages of embryonic development of the zebrafish. *Dev. Dyn.* **203**, 253-310.

Kimmel, C.B., Warga, R.M. and Kane, D.A. (1994). Cell cycles and clonal strings during formation of the zebrafish central nervous system. *Development* **120**, 265-276.

Lowery, L.A., De Rienzo, G., Gutzman, J.H. and Sive, H. (2009). Characterization and classification of zebrafish brain morphology mutants. *Anat. Rec*. **292**, 94-106

Lowery, L.A. and Sive, H. (2005). Initial formation of zebrafish brain ventricles occurs independently of circulation and requires the nagie oko and snakehead/atp1a1a.1 gene products. *Development* **132**, 2057-2067.

Martin-Belmonte, F. and Mostov, K. (2008). Regulation of cell polarity during epithelial morphogenesis. *Curr. Opin. Cell Biol.* **20**, 227-34.

McGill, M.A., McKinley, R.F. and Harris, T.J. (2009). Independent cadherin-catenin and Bazooka clusters interact to assemble adherens junctions. *J. Cell Biol.* **185**, 787-96.

Morais-de-Sa, E., Mirouse, V. and St Johnston, D. (2010). aPKC phosphorylation of Bazooka defines the apical/lateral border in Drosophila epithelial cells. *Cell* **141**, 509-523.

Pilot, F., Philippe, J.M., Lemmers, C. and Lecuit, T. (2006). Spatial control of actin organization at adherens junctions by a synaptotagmin-like protein Btsz. *Nature* **442**, 580-584.

Pinheiro, D and Bellaiche, Y. (2018). Mechanical force-driven adherens junction remodeling and epithelial dynamics. *Dev. Cell* **47**,3-19.

Rathbun, L.I., Colicino, E.G., Manikas, J., O'Connell, J., Krishnan, N., Reilly, N.S., Coyne, S., Erdemci-Tandogan, G., Garrastegui, A., Freshour, J., Santra, P., Manning, M.L., Amack, J.D. and Hehnly, H. (2020). Cytokinetic bridge triggers de novo lumen formation in vivo. *Nat.. Commun.* **11**, 1269.

Revenu, C., Streichan, S., Donà, E., Lecaudey, V., Hufnagel, L. and Gilmour, D. (2014). Quantitative cell polarity imaging defines leader-to-follower transitions during collective migration and the key role of microtubule-dependent adherens junction formation. *Development* **141**, 1282-1291.

Roeth, J.F., Sawyer, J.K., Wilner, D.A. and Peifer, M. (2009). Rab11 helps maintain apical crumbs and adherens junctions in the Drosophila embryonic ectoderm. *PLoS One* **4**, e7634.

Roh, M.H., Makarova, O., Liu, C.J., Shin, K., Lee, S., Laurinec, S., Goyal, M., Wiggins, R. and Margolis, B. (2002). The Maguk protein, Pals1, functions as an adapter, linking mammalian homologues of Crumbs and Discs Lost. *J. Cell Biol.* **157**, 161-172.

Sarov, M., Schneider, S., Pozniakovski, A., Roguev, A., Ernst, S., Zhang, Y., Hyman, A.A. and Stewart, A.F. (2006). A recombineering pipeline for functional genomics applied to Caenorhabditis elegans. *Nat. Methods* **3**, 839-844.

Schoenwolf, G.C. (1984). Histological and ultrastructural studies of secondary neurulation of mouse embryos. *Am. J. Anat.* **169**, 361–374.

Schwayer, C., Shamipour, S., Pranjic-Ferscha, K., Schauer, A., Balda, M., Tada, M., Matter, K. and Heisenberg, C.P. (2019). Mechanosensation of tight junctions depends on ZO-1 phase separation and flow. *Cell* **179**, 937-952.

St Johnston, D. and Ahringer, J. (2010). Cell polarity in eggs and epithelia: Parallels and diversity. *Cell* **141**, 757-774.

Suster, M.L., Abe, G., Schouw, A. and Kawakami, K. (2011). Transposon-mediated BAC transgenesis in zebrafish. *Nat. Protoc*. **6**, 1998-2021.

Tait, C.M., Chinnaiya, K., Manning, E., Murtaza, M., Ashton, J.P., Furley, N., Hill, C.J., Alves, C.H., Wijnholds, J., Erdmann, K.S., Furley, A., Rashbass, P., Das, R.M., Storey, K.G. and Placzek, M (2020). Crumbs2 mediates ventricular layer remodelling to form the spinal cord central canal. *PLoS Biol*. **18**, e3000470.

Tawk, M., Araya, C., Lyons, D.A., Reugels, A.M., Girdler, G.C., Bayley, P.R., Hyde, D.R., Tada, M. and Clarke, J.D. (2007). A mirror-symmetric cell division that orchestrates neuroepithelial morphogenesis. *Nature* **446**, 797-800.

Tepass, U. (1996). Crumbs, a component of the apical membrane, is required for zonula adherens formation in primary epithelia of Drosophila. *Dev. Biol.* **177**, 217-225.

Thisse, B. and Thisse, C. (2004). Fast release clones: A high throughput expression analysis. ZFIN Direct Data Submission.

Thompson, B.J., Pichaud, F. and Röper, K. (2013). Sticking together the Crumbs - an unexpected function for an old friend. *Nat. Rev. Mol. Cell Biol.* **14**, 307-314.

von Trotha, J.W., Campos-Ortega, J.A. and Reugels, A.M. (2006). Apical localization of ASIP/PAR-3:EGFP in zebrafish neuroepithelial cells involves the oligomerization domain CR1, the PDZ domains, and the C-terminal portion of the protein. *Dev. Dyn*. **235**, 967-977.

Wei, S.Y., Escudero, L.M., Yu, F., Chang, L.H., Chen, L.Y., Ho, Y.H., Lin, C.M., Chou, C.S., Chia, W., Modolell, J. and Hsu, J.C. (2005). Echinoid is a component of adherens junctions that cooperates with DE-Cadherin to mediate cell adhesion. *Dev. Cell* **8**: 493-504.

Wei, X. and Malicki, J. (2002). nagie oko, encoding a MAGUK-family protein, is essential for cellular patterning of the retina. *Nat. Genet.* **31**, 150-157.

Westerfield, M. (2000). *The zebrafish book. A guide for the laboratory use of zebrafish (Danio rerio).* Univ. of Oregon Press, Eugene.

Yang, X., Zou, J., Hyde, D.R., Davidson, L.A. and Wei, X. (2009) Stepwise Maturation of Apicobasal Polarity of the Neuroepithelium Is Essential for Vertebrate Neurulation. *J. Neurosci***. 29,** 11426-11440.

Zou, J., Wen, Y., Yang, X. and Wei, X. (2013). Spatial-temporal expressions of Crumbs and Nagie oko and their interdependence in zebrafish central nervous system during early development. *Int. J. Dev. Neurosci.* **31**, 770-782.

Figure Legends

Figure 1. Nok dependent spot adhesion to apical ring transition.

A) Diagram of neural rod with inserted red sheet to illustrate sagittal plane of confocal sections. Red arrow indicates direction of imaging.

B) Sagittal confocal planes of neural rod in anterior spinal cord region at 11, 13, 15 and 17 somite stages. Comparable images were seen at each timepoint from 3 embryos. Bottom row images are from fixed embryos stained for Zonula Occludens 1 (ZO-1). Comparable images were seen from 2 embryos at each timepoint. Red arrow indicates ventral apical rings and red arrowheads indicates puncta. Dorsal to the top of each panel.

C) Sagittal confocal images at 12 somite stage showing Pard3-EGFP puncta are often located at cell vertices (arrowed, n = 8 embryos). Plasma membrane imaged using mNeptune2.5-CAAX (mNept-CX).

D Examples of punctate Pard3-EGFP in developing apical rings from a 15 somite stage embryo. Dorsal example shows an immature, incomplete ring. Ventral example shows a more complete ring, with arrows indicating multiple puncta between vertices. Single sagittal confocal planes.

E) A heat-map quantification of the formation of mature Pard3 apical rings from two embryos over developmental time and dorsoventral position.

F) Parasagittal confocal sections from left hand side (LHS) and right-hand side (RHS) of stage 15 somite neural rod. Incomplete apical rings of Pard3-EGFP are forming independently on left and right sides of the midline.

G) Parasagittal and sagittal confocal sections at 17 somite stage showing complete apical rings of Pard3-EGFP on either side of the midline. The sagittal section (labelled Middle) shows a largely diffuse low level of Pard3-EGFP expression in the midline territory between the left and right rings (see supplementary movie 1).

Apical ring formation in F & G analysed from over 10 embryos. For each embryo, 10-25 apical rings were located on one side of the neuroepithelium and a z-stack was taken through the middle of the neural rod until the rings on the opposite side were visible.

H) Images taken from confocal time-lapse movies of wild-type and *nok* morphant Pard3-EGFP embryos in sagittal orientation from the 16 somite stage to 24 hpf. Comparable images were seen from 3 embryos from each genotype. Three control morphants were also assessed in the Cdh2-tFT transgenic line and all had comparable apical rings to wild types.

Figure 2. Sister-cells remain attached via their corners

A) Images from time-lapse movie projection in dorsal orientation of mosaically labelled neuroepithelial cells in the hindbrain of an 11 somite stage WT embryo. Membrane and nuclei

are labelled in magenta. By the 13 somite stage, both cells had undergone C-division, resulting in pairs of sister cells attached across the tissue midline. The top cell pair was followed over time until the 18 somite neural rod stage, when both cell pairs were imaged. The configuration of cell pair connections was assessed from several different experiments at the neural rod stage (approximately 16-18 somites) and 26/31 pairs of cells from 5 embryos at neural rod stages were found to be clearly attached via their corners. The remaining 5 were either connected via a more 'en face' configuration or their configuration was uncertain (e.g. due to a very thin connection point).

B) i. Single z-planes from a time-lapse movie of a C-division (yellow cell) starting at the 10 somite stage (neural keel) from a Cdh2-tFT transgenic embryo. The image contrast was increased in the reference image at the top to highlight that Cdh2 was concentrated at the interdigitation zone between cells around the tissue midline at 0 minutes. Cdh2-GFP becomes strongly concentrated in the cleavage furrow (timepoint 15 min) and neighbouring cells ingress into the cleavage furrow (21/21 divisions, red arrows). In this example the pink cell that ingresses into the cleavage furrow gains a contralateral contact with the contralateral daughter of the C-division. Because of this contact, the contralateral daughter (yellow cell on right) becomes attached to two contralateral cells – one is its sister cell from the C-division and the other is one of its sister's neighbouring cells (the pink cell in this example).

ii. 5 µm projection of 17 somite stage neural rod from a Cdh2-tFT transgenic embryo. Endfeet are aligned along a centrally located midline. Cdh2-GFP is upregulated along the midline, particularly at cell corners (red arrowheads in magnified region).

iii. Model depicting the co-ingression of neighbouring cells into the cleavage furrow during C-division (yellow cells) and the subsequent offsetting of sister cells from each other, which precedes apical ring formation. Based on the images similar to those in Figure Bi. Pink lines and dots represent high levels of Cdh2 associated with the dividing cell. The ingression of either ipsilateral (e.g. orange) or contralateral (e.g. blue) neighbours into the cleavage furrow promotes the formation of multiple contralateral connections across the midline. For example, the left-hand yellow sister cell becomes attached to both its right-hand yellow sister cell and the ingressing blue cell. The right-hand yellow sister cell becomes attached to both its left-hand yellow sister cell and the ingressing orange cell.

C) i. Transmission electron micrographs of a 20 hpf embryo hindbrain in transverse orientation. The lumen has just started to open from the midline. The interface between contralateral cells has a striking 'zig-zag' pattern (3/3 19-20 hpf embryos). **ii.** Inset magnified region from **i**.

Figure 3. Nok dependent remodelling of midline adhesions.

A) i. Images from confocal time-lapse movies of Pard3-EGFP and Cdh2-GFP embryos in horizontal orientation at 11 somite, 17 somite and 24 hpf stages. Comparable images were seen from 3 embryos from each transgenic line.

ii and **iii.** Mean intensity profiles from 6 embryos, quantifying Pard3 intensity across the basal-to-basal width of the developing neuroepithelium over time, starting at the 16 somite stage. Standard deviation is shown as a grey ribbon around the line profile for each timepoint in **iii.**

iv. Mean intensity profiles from the same 6 embryos, quantifying Pard3 intensity across the basal-to-basal width of the neuroepithelium at the fully neuroepithelial stage.

v. Horizontal confocal planes of 17 somite stage neural rod showing Pard3-EGFP expression at five different dorsoventral levels. The single elevated plane of expression at the left right interface seen at level 17 µm, lies dorsal to levels where apical rings are already formed and ventral to levels where expression is more prominent in mediolateral streaks.

vi. Single horizontal plane confocal section of Pard3-EGFP and mNeptune2.5-CAAX and merge at approximately 24 hpf. Plasma membranes meet at the tissue midline while Pard3 is now largely located in two parallel parasagittal domains.

B) Horizontal and transverse confocal sections of 30 hpf. **i.** wild-type and **ii.** *nok*^{m227} mutant Cdh2-GFP embryos at the hindbrain level. The hindbrain lumen remained closed in 5/5 *nok*^{m227} mutant embryos and is always open in wild types.

C) Horizontal confocal sections of **i.** wild-type and **ii.** *nok*^{m227} mutant Cdh2-GFP embryos at the anterior spinal cord level, stained for Crb2a. Insets in the 18 and 26 somite stages of wildtypes show merge of Crb2a and Cdh2-GFP expression. **i.** In wild-type embryos, Cdh2 and Crb2a were colocalised at the midline at 18 somite stage (4/4 embryos) but Cdh2-GFP was displaced basolaterally to form two independent stripes of expression either side of the midline by the 26 somite stage (8/8 embryos). In *nok*^{m227} mutants, Crb2a was not present at the midline at the 18 somite stage (4/4 embryos) and Cdh2-GFP remained in a single expression domain at the tissue midline even as late as 28 hpf (5/5 embryos).

Figure 4. Persistent adhesion in Nok and Rab11a deficient cells

A) Images from time-lapse movie of mosaically labelled neuroepithelial cells in the hindbrain of a 30 hpf WT embryo, dorsal view. Cells have separated across the tissue midline and the lumen has opened (short dotted lines). D-divisions (stars) occur at the apical surface and cells re-established an elongated morphology towards the basal surface following division.

B) Images from time-lapse movie of mosaically labelled neuroepithelial cells in the hindbrain of a 30 hpf *nok* morphant embryo, dorsal view. Cells have failed to separate across the tissue midline (dotted line) and formed clumps (sometimes with a rosette-like structure, arrow). D-

divisions (stars) occurred near the centre of the cell clumps, which was often not situated near the tissue midline. Of 117 daughter cells followed post division, at least 40% did not fully re-extend to the basal side of the neural rod.

C) Graph of cell division locations in relation to the tissue midline or lumen edge over development. 71 cells were analysed from 3 *nok* morphant embryos. In embryos over 25 hpf, 49% of *nok* morphant cells divided 5µm or more away from the midline. Division locations from a single wild type embryo example are included in black.

D) A 10 µm z-projection, dorsal view, at mid dorso-ventral level through the hindbrain of *nok* morphant Pard3-EGFP embryos at 22 hpf and 48 hpf. At 22 hpf Pard3-EGFP was localised near the tissue midline but did not form continuous straight expression domains as seen in wild types (Figure 3Ai) and the lumen failed to open. By 48 hpf Pard3-EGFP localisation became fragmented into clumps. 9/9 *nok* mutant embryos and 6/8 *nok* morphant embryos over 24 hpf old from 5 different experiments had fragmented midlines and ectopic apical proteins. The extent of this disorganisation was greater in older embryos. 2/8 *nok* morphant embryos had a milder phenotype, (see supplementary figure 1). 9/9 wild type embryos had normal apical surfaces with no ectopic apical proteins.

E) 70-80 µm maximum projections, dorsal view of hindbrain at 19 hpf, stained for Crumbs 1 (Crb1) and ZO1. **i.** Wild-type embryo. Both Crb1 and ZO1 were localised to the apical midline (n=3/3). **ii.** Embryo in which UAS:DNRab11a was expressed under the Krox20:KalTA4 activator in rhombomeres 3 and 5. ZO1 localised to the midline but Crb1 was largely absent from rhombomeres 3 and 5 (n=3/3).

F) i. 11 µm maximum projection dorsal view of hindbrain neuroepithelial cells at 20 hpf in DNRab11a x Krox20 embryo. Magenta shows DNRab11a rhombomere 5. Lumen in rhombomere 5 failed to open but had opened in rhombomeres 4 and 6 (short dashed lines). Note, obscuring overlying cells in different z-planes were removed from the images.

ii. Images from time-lapse movie of cells in i, which failed to separate across the tissue midline (white dashes). Similar to *nok* morphant embryos (Figure 4B), following D-divisions (stars), cells remained attached and were arranged into a rosette-like structure (arrow), enlarged in **iii**. Cell clumping or rosette-like structures observed in DNRab11a rhombomeres of all 9 embryos analysed from 3 experiments.

G) Time-lapse reconstruction showing mosaically distributed DNRab11a-EGFP neuroepithelial cells in hindbrain of 24 somite stage (21 hpf) embryo. Following D-divisions (stars), cells did not separate and formed a rosette around centrally located puncta of Pard3-RFP.

H) 70 µm maximum projections from time-lapse movie through a DNRab11a x Krox20 embryo hindbrain labelled with Pard3-EGFP, starting at 24 hpf. As in *nok* morphants in figure 4D, Pard3 was initially close to midline of rhombomere 5, but the lumen failed to open and Pard3 localisation became fragmented into clumps that dispersed over time (17/17 embryos).

I) 4 µm maximum projection, dorsal view of 30 hpf DNRab11a x Krox20 embryo rhombomere 3, stained for Pard3 and gamma-tubulin. Pard3 is localised in a round clump, surrounded on all sides by centrosomes.

J) DNRab11a rhombomeres 3 and 5 had approximately 7 ectopic clumps of Pard3 and gamma-tubulin at 30 hpf (n=4 embryos. Error bars denote standard deviations). No ectopic clumps in wild-type rhombomeres.

Figure 5. Cells at the WT/DNRab11a interface contribute to the luminal surface

A) 15-18 µm maximum projections through 32 hpf DNRab11a x krox20 embryo hindbrains stained for Crb2a (i) or aPKC (ii). Cells mosaically labelled with cytoplasmic GFP and H2A-GFP.

i. Crb2a is largely absent from DNRab11a cells (blue) contacting lumen (5/5 embryos).

ii. aPKC is present at lumen in both wild-type and DNRab11a cells (blue) (4/4 embryos). Cells in the centre of DNRab11a rhombomeres clumped together (e.g. star in i) whilst cells in contact with the open lumens had elongated morphology (e.g. arrows in ii).

B) Single dorsal view z-slices from time-lapse movie of neuroepithelial cells in rhombomere 5 of a 24 hpf DNRab11a x Krox20 embryo. Long dotted lines denote basal surfaces. Short dotted lines denote apical surfaces.

i) As the neighbouring lumen inflated, cells at the edge of the DNRab11a rhombomere remained connected across the midline and cells near the edge divided at this central point of connection with parallel orientation (star).

ii) As the neighbouring lumen inflated further, cells near the WT/DNRab11a interface reoriented towards the open lumen (e.g. arrows). Cells divided at the opening luminal surface with parallel orientation (stars). This widened the DNRab11a luminal surface further (see measurements in orange).

iii) Quantification of cell division orientation. 104 DNRab11a cell divisions were analysed from 3 embryos over the 24-40 hpf period of development. 87% of DNRab11a cells dividing at the luminal edge did so parallel to the opening lumen, whilst 38% of DNRab11a cells dividing in the middle of rhombomeres 3 and 5 did so parallel to the midline (P=0.0121, unpaired, 2-tailed t-test). Error bars denote standard deviations between embryos.

Figure 6. Nok is necessary for apical ring formation even in absence of cell division.

All embryos are at 28 somite stage. **A-D)** Orthogonal series of horizontal (top left), transverse (top right) and sagittal (bottom) confocal planes of Pard-EGFP expression in the following embryos:

A) wildtype sibling treated with DMSO vehicle control. Many small apical rings have formed at tissue midline (n=3/3 embryos).

B) wildtype sibling treated with aphidicolin to block the C-divisions**.** Fewer, large apical rings have formed at the tissue midline (n=4/4 embryos).

C) *nok*^{m227} mutant embryo treated with DMSO vehicle control. No apical rings have formed at the tissue midline. Pard3 is visible as spots along the midline plane (n=3/3 embryos).

D) *nok*^{m227} mutant embryo treated with aphidicolin to block C-divisions. No apical rings have formed at the tissue midline. Pard3 is visible as spots along the midline plane (n=4/4 embryos).

E) Overall body shape of wildtype siblings and *nok*^{m227} mutants with and without aphidicolin treatment.

F) Horizontal section through neural tube showing nuclear staining in wildtype embryos treated with DMSO or aphidicolin to block C-divisions. Aphidicolin-treated embryo have larger nuclei, demonstrating that S-phase division-block was successful.

G) Quantification of nucleus area of wildtype siblings and *nok*^{m227} mutants with and without aphidicolin treatment. Data from 100-150 nuclei pooled from 2-3 embryos in each group and analysed by 2-way ANOVA. Areas of Aphidicolin treated nuclei were, on average, 30 μm^2 bigger than DMSO treated embryos ($P<0.0001$). No significant difference in nuclei area between wild type and *nok*^{m227} mutant embryos ($P=0.8561$). Error bars denote standard deviations.

H) Quantification of apical ring number in wildtype siblings and *nok*^{m227} mutants with and without aphidicolin treatment. Numbers of apical rings per 1000 μm^2 calculated from 3-4 embryos per group. No apical rings were seen in any of the *nok*^{m227} mutants. There were, on average, 40 fewer apical rings per 1000 μm^2 in aphidicolin treated wild type embryos than in DMSO treated wild type embryos (unpaired t-test, $P=0.0222$). Error bars denote standard deviations.

A

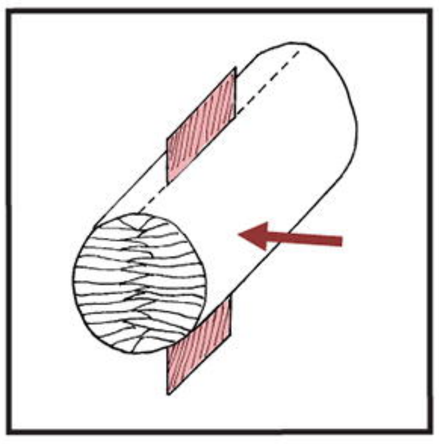

B

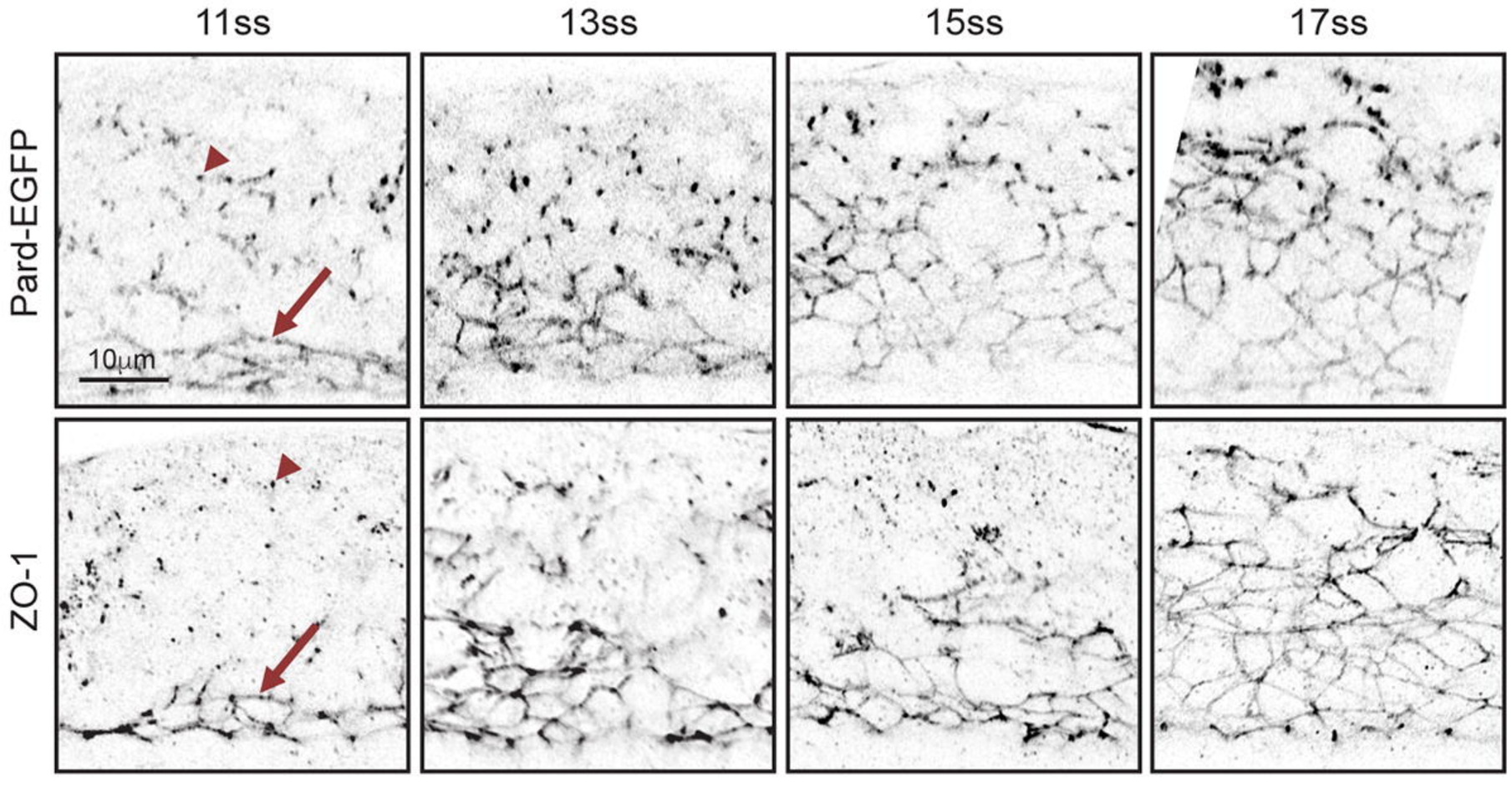
11ss
13ss
15ss
17ss
Pard-EGFP
ZO-1
10μm

C

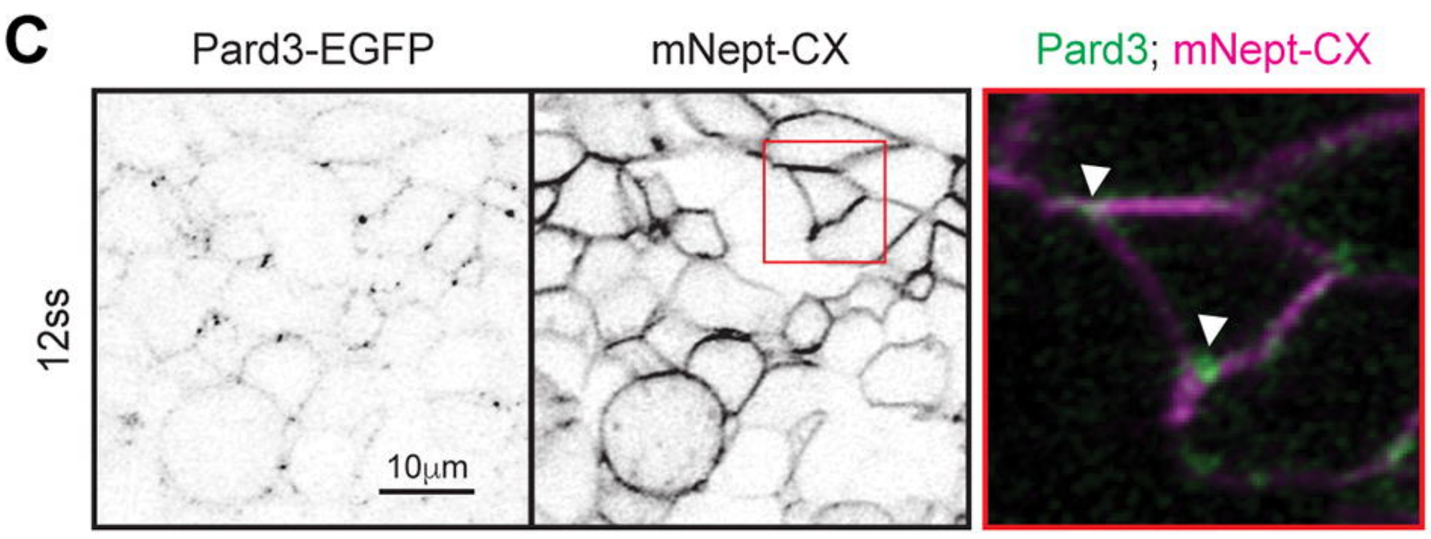
Pard3-EGFP
mNept-CX
Pard3; mNept-CX
12ss
10μm

D

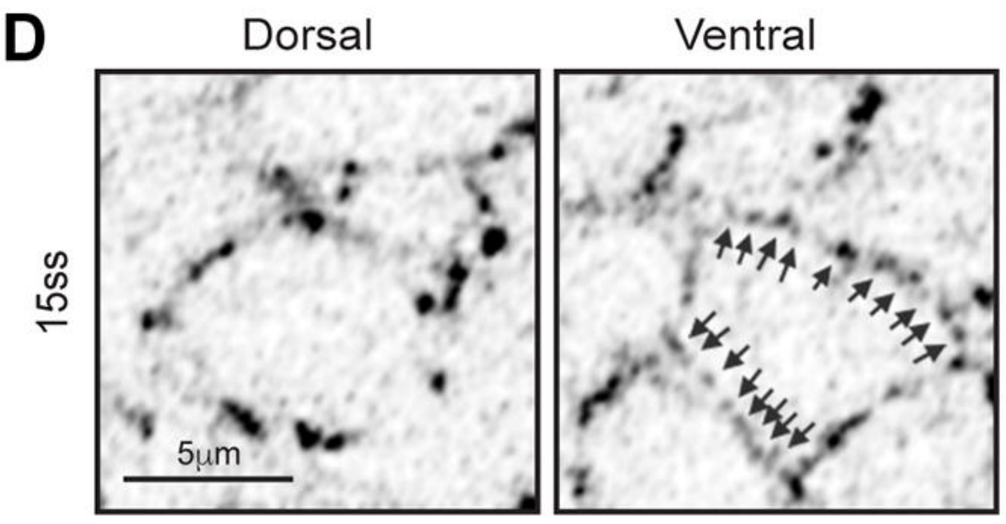
Dorsal
Ventral
15ss
5μm

E

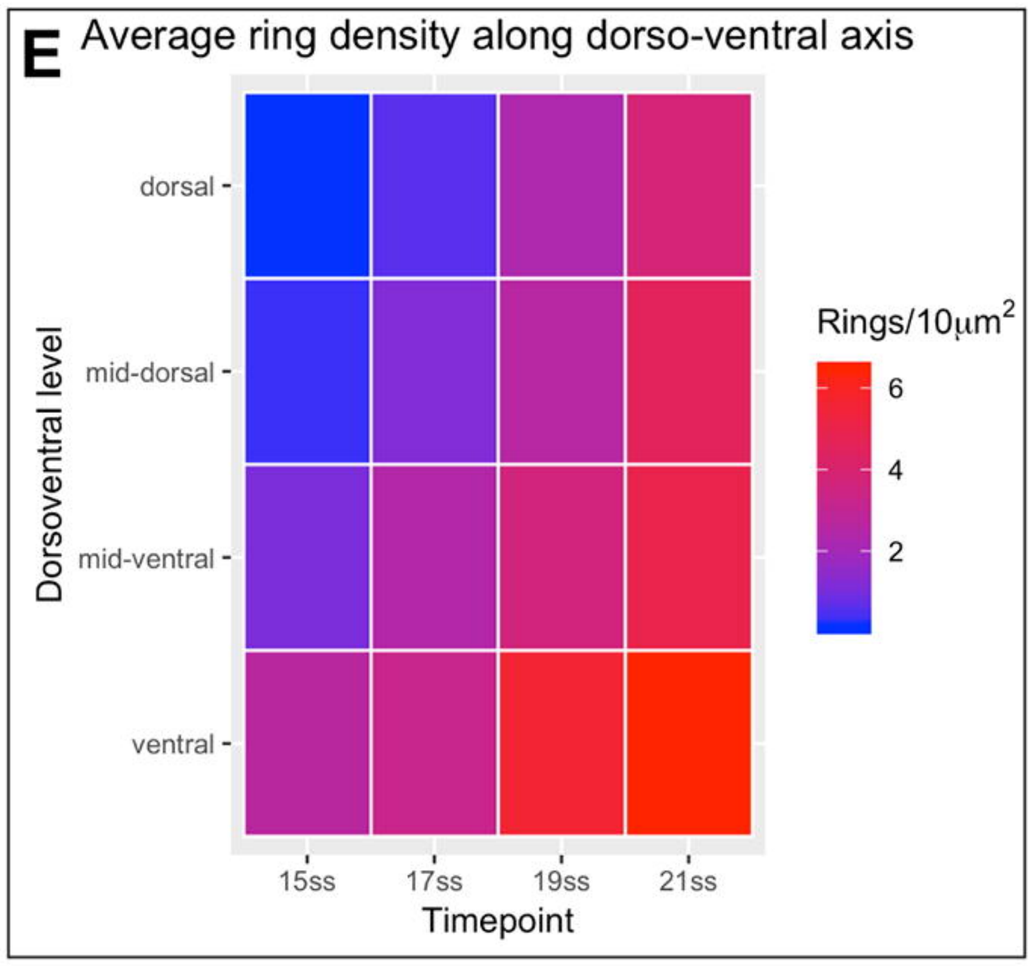
Average ring density along dorso-ventral axis
dorsal
mid-dorsal
mid-ventral
ventral
Dorsoventral level
15ss
17ss
19ss
21ss
Timepoint
Rings/10μm2
6
4
2

F

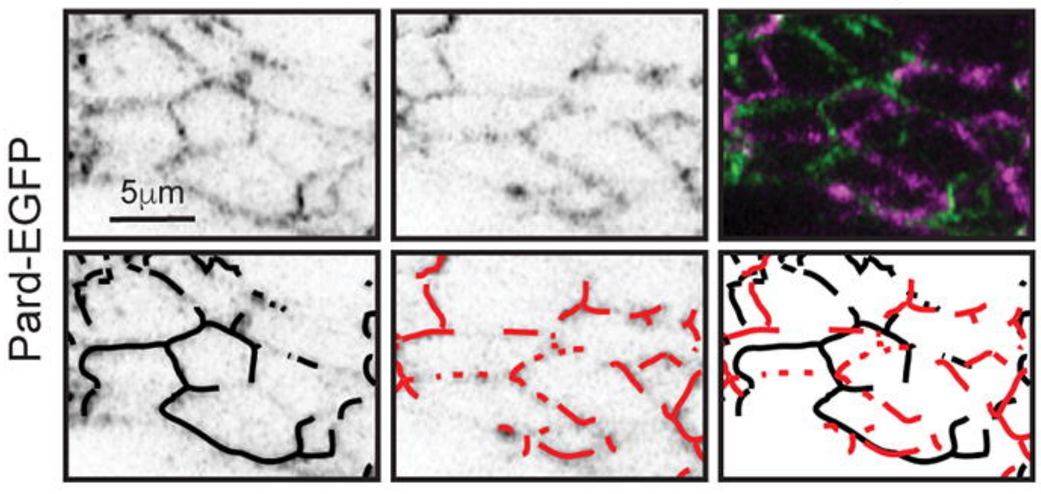
LHS
RHS
Merge
Pard-EGFP
5μm

G

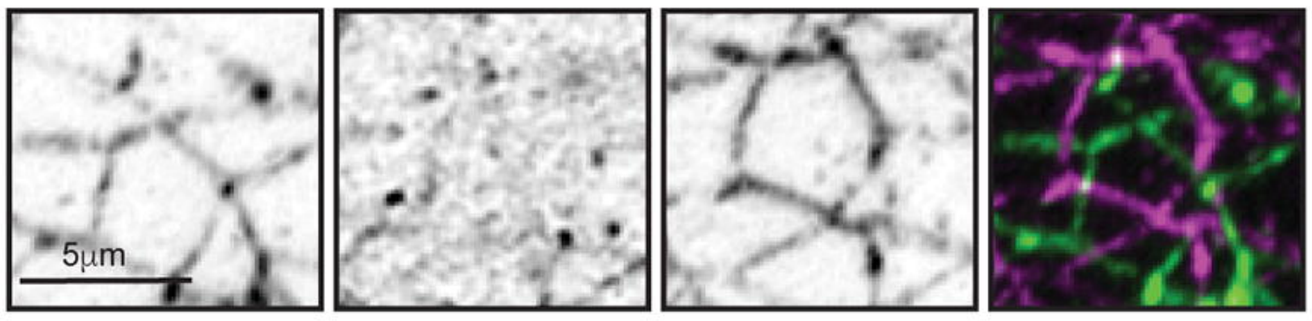
LHS
Middle
RHS
Merge
5μm

H

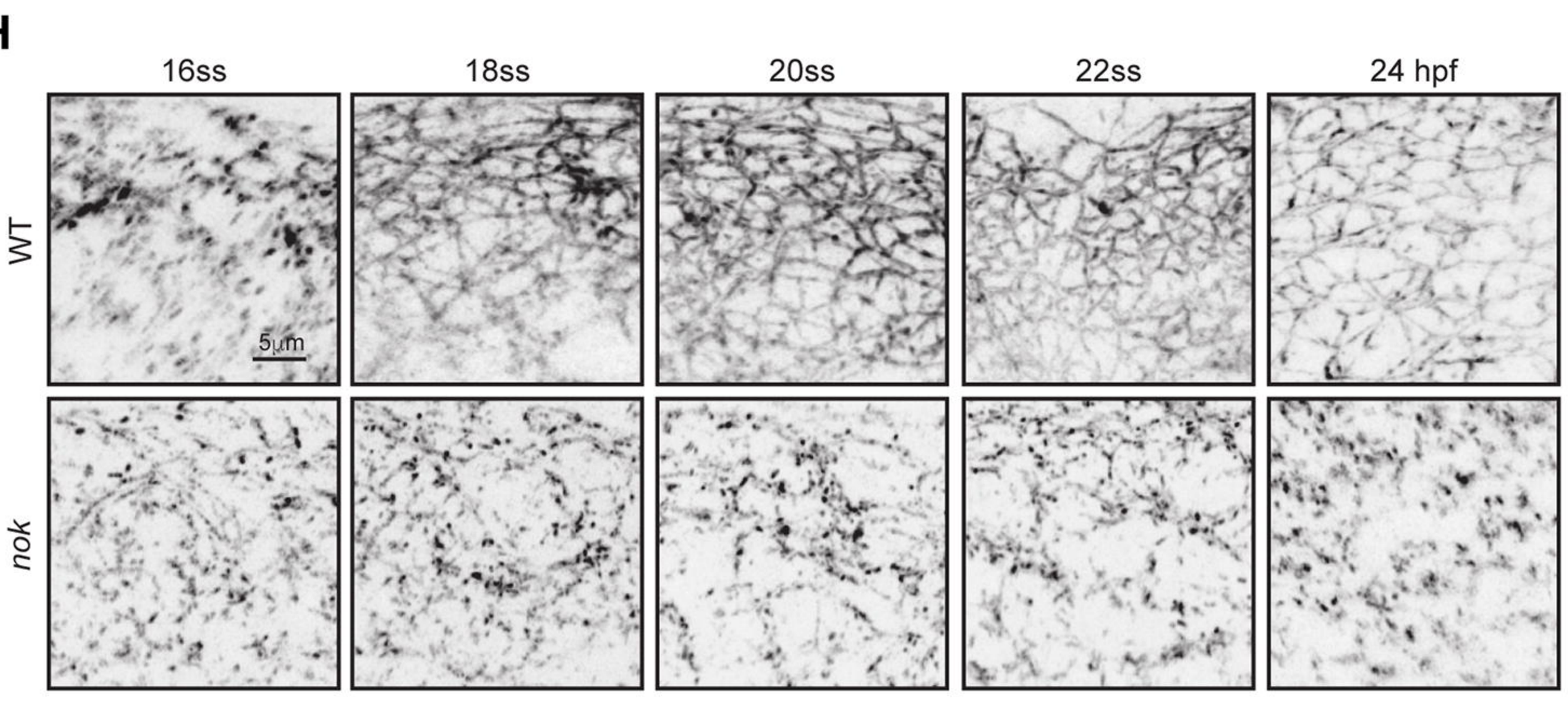
16ss
18ss
20ss
22ss
24 hpf
WT
nok
5μm

A

11 somites

10μm

13 somites

+ 1 min 30 secs

+ 5 mins

14 somites

+ 19 mins

15 somites

18 somites

Bi

Cdh2-tFT, 10 somites

5μm

0 mins

+ 11 mins

+ 15 mins

+ 16 mins

+ 20 mins

+ 23 mins

+ 45 mins

iii

Early neural keel. Progenitor cells interdigitated

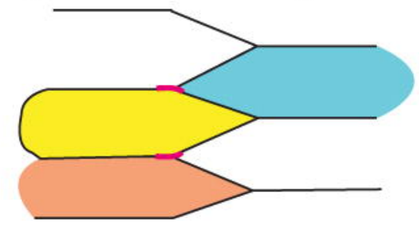

C-division. Progenitor cell rounds up near the tissue midline

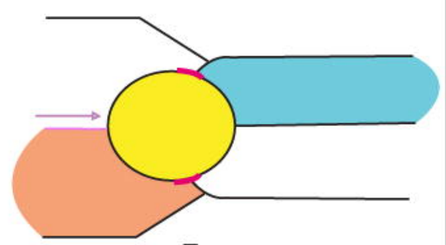

C-division. Neighbouring cells ingress into cleavage furrow

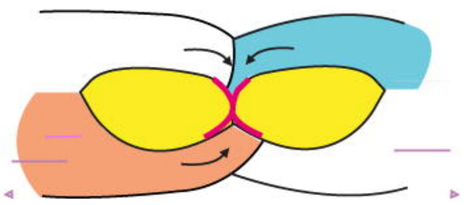

Later neural keel. Sister cells start to become offset from each other

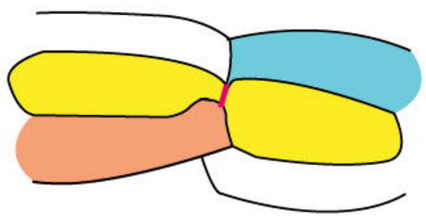

Neural rod. Maintenance of cell connections during alignment of apical endfeet at the midline would lead to offset configuration of sister cells. Apical rings form independently (see figure 1)

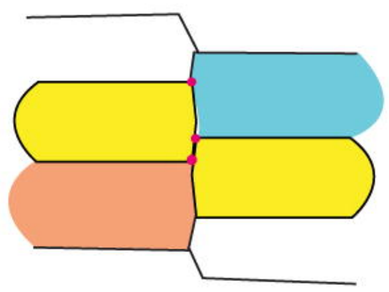

Ci

ii

1μm

10μm

ii

17 somites

5μm

5μm

Ai
11ss
17ss
24 hpf
Pard3
Cdh2
10μm
ii
Mean intensity (A.U.)
Distance (μm)
0h
1h
2h
3h
iii
16 ss
+1h
+2h
+3h
Mean intensity (A.U.)
Distance (μm)
iv
Fully neuroepithelial
Ventral
Dorsal
v
Pard3
0μm
13μm
17μm
25μm
26μm
10μm
vi
Pard3
CAAX
Merge
10μm
B
30 hfp, dorsal view
30 hpf, trans section
30 hpf, dorsal view
30 hpf, trans section
i
Cdh2
WT
50μm
50μm
ii
nok
50μm
50μm
C
17ss
18ss
26ss
18ss
28 hpf
i
Cdh2
5μm
Crb2a
WT
ii
nok

A
WT
30 h.p.f.
+ 1 hours, 40 mins
+ 4 hours, 10 mins
10μm
B
nok morphant
30 h.p.f.
+ 50 mins
+ 2 hours, 10 mins
10μm
C
Distance from tissue midline /lumen edge (μm)
h.p.f.
WT embryo
nok embryo 1
nok embryo 2
nok embryo 3
D
nok morphant
Pard3-EGFP
22 h.p.f.
10μm
48 h.p.f.
F
Rab11aDN x Krox20
i
R4
R5
R6
otycyst
otycyst
10μm
~20 h.p.f.
ii
~20 h.p.f.
+ 45 mins
iii
E
WT
i
Crb1
R5
19 h.p.f.
30μm
ZO1
R5
Rab11aDN x Krox20
ii
Crb1
R3
R5
ZO1
R3
R5
G
DNRab11a-EGFP, Pard3-RFP
10μm
21 h.p.f.
+ 1 hour 20 mins
+ 1 hour 40 mins
+ 2 hour 50 mins
Rab11aDN x Krox20
Hi
R4
Pard3-EGFP
R5
10μm
R6
~24 h.p.f.
ii
~30 h.p.f.
iii
~33 h.p.f.
I
gamma tublin, Pard3
R3
10μm
30hpf
J
Ectopic clumps
R3
R5

Rab11aDN x Krox20, 32hpf

A

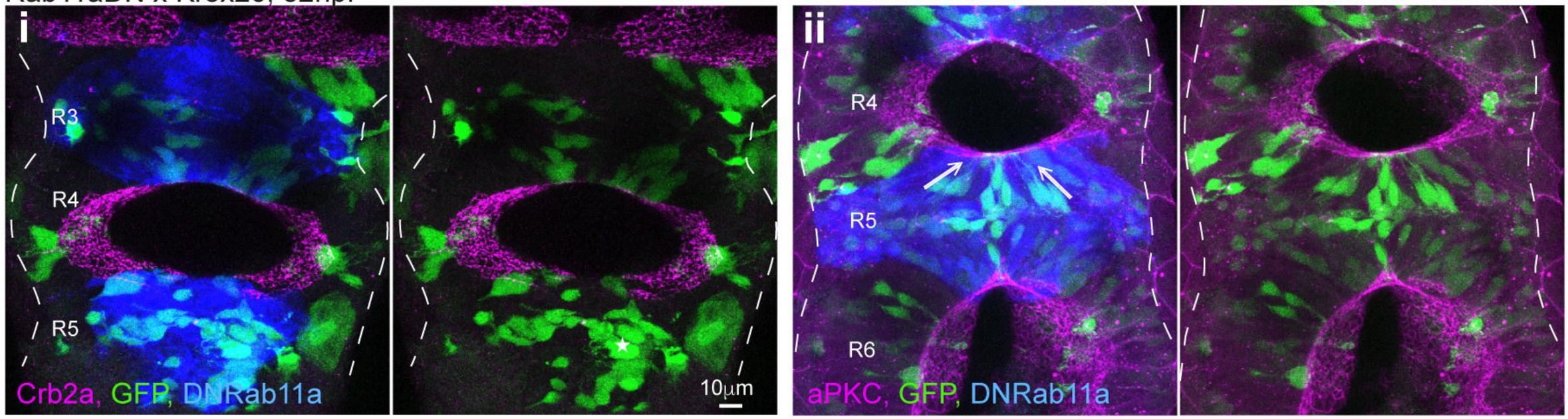

Bi

Rab11aDN x Krox20, ~24hpf

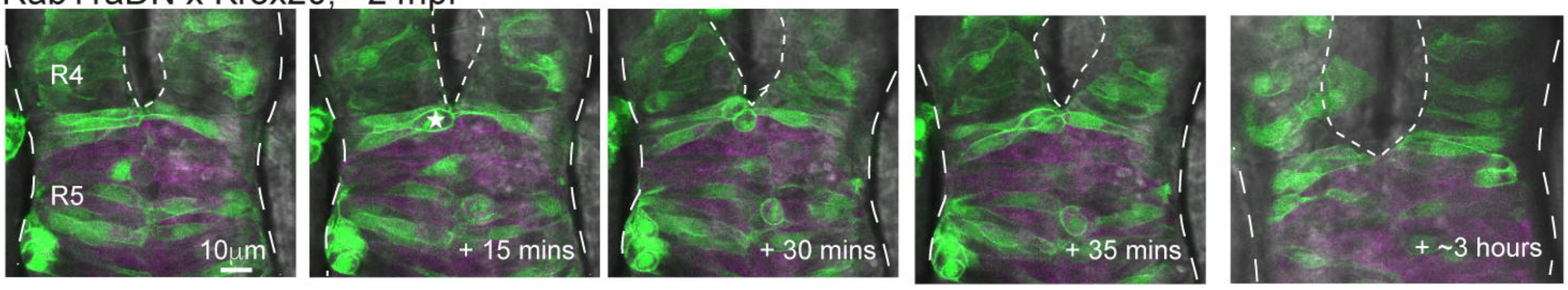

Biii

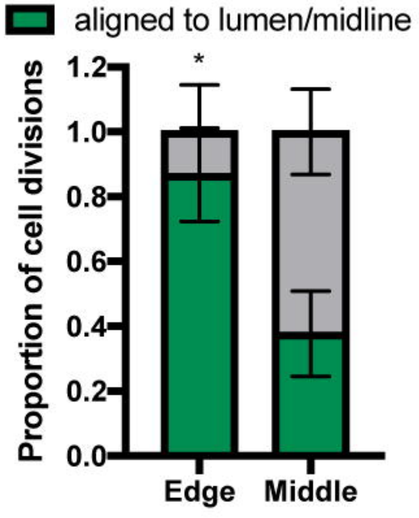

ii

Rab11aDN x Krox20, ~31hpf

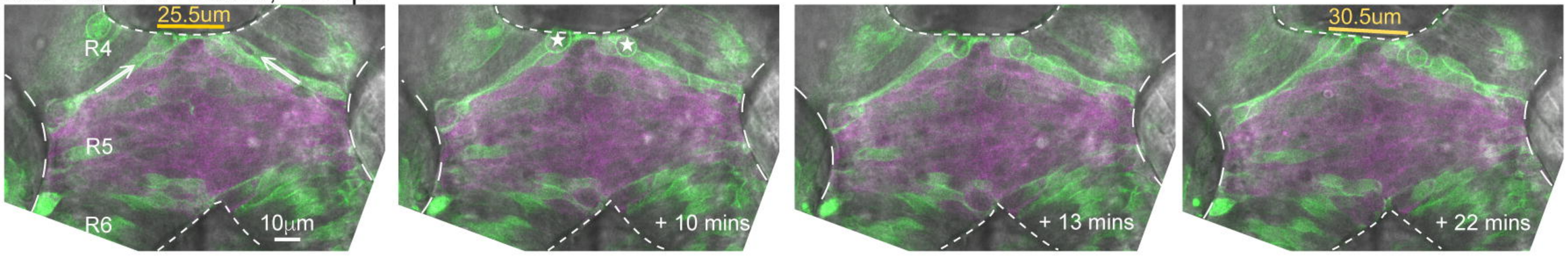

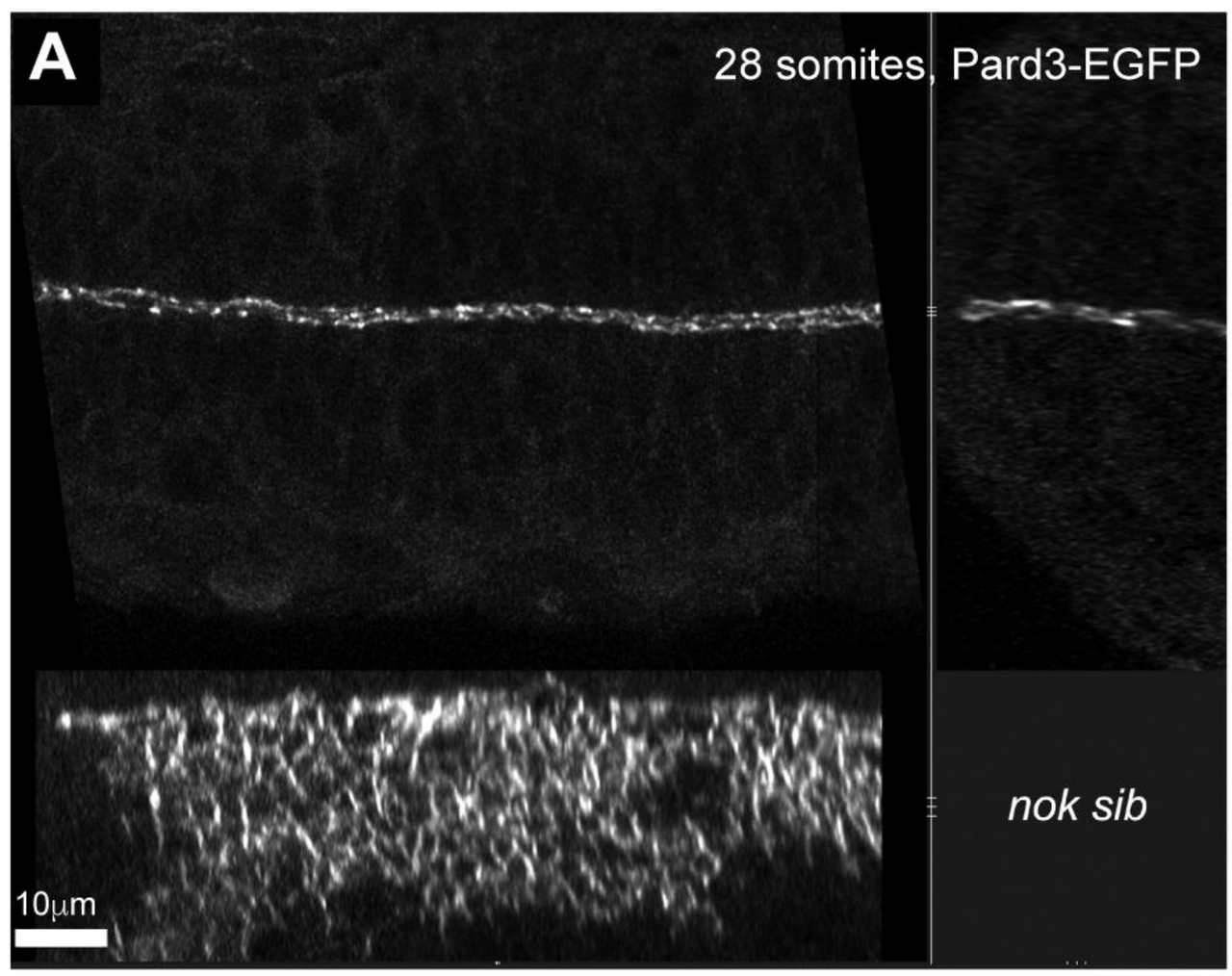
A
28 somites, Pard3-EGFP
nok sib
10μm

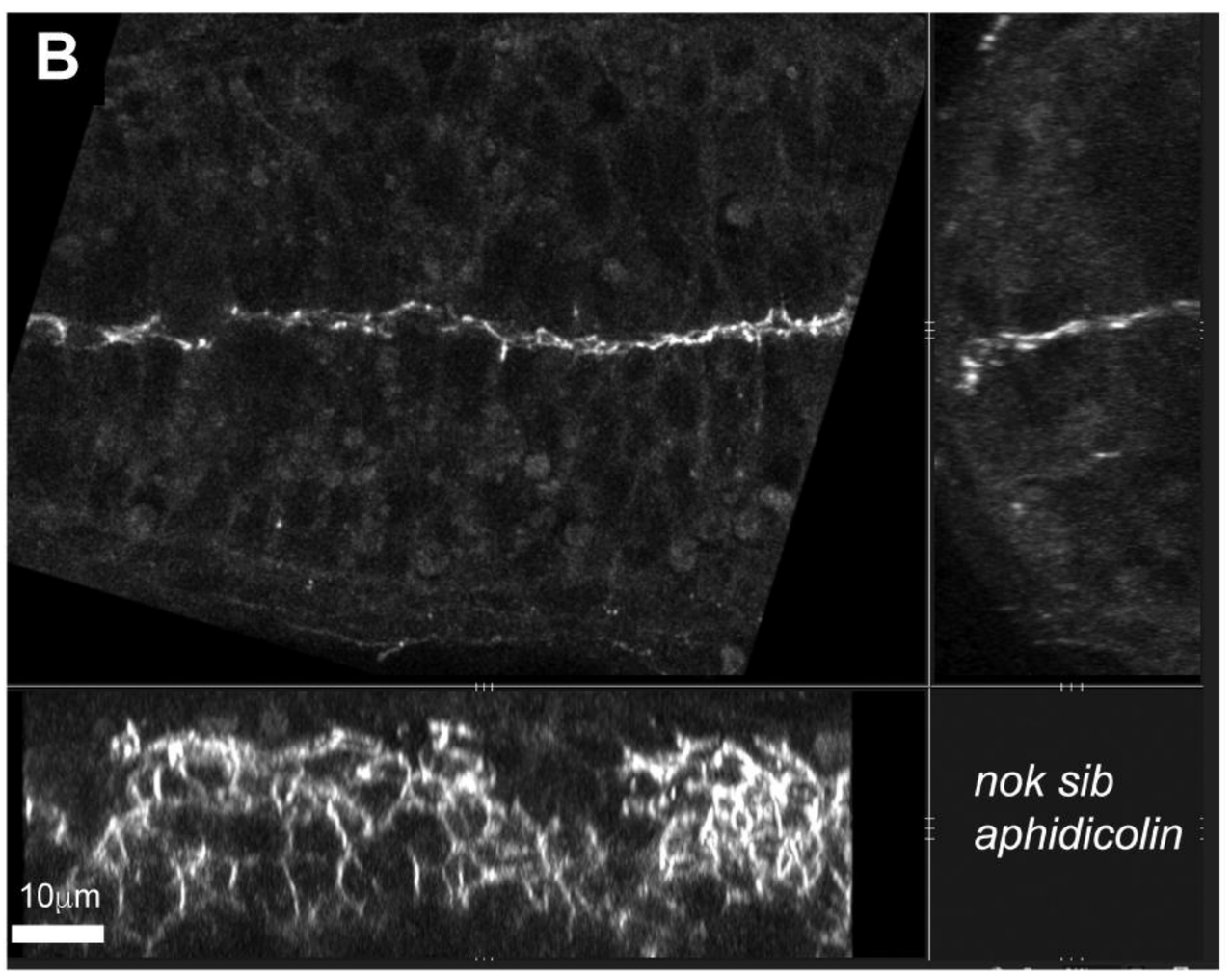
B
nok sib
aphidicolin
10μm

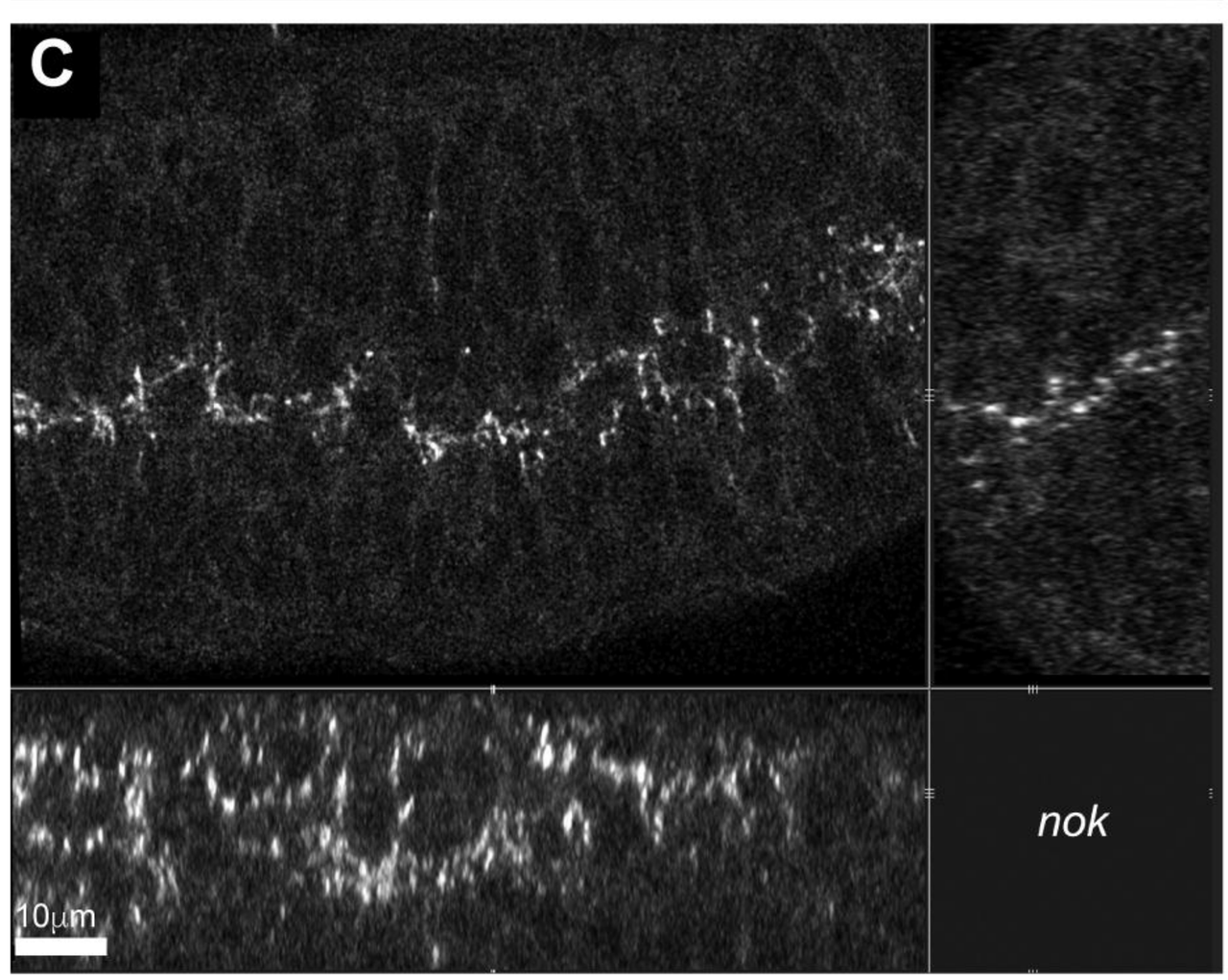
C
nok
10μm

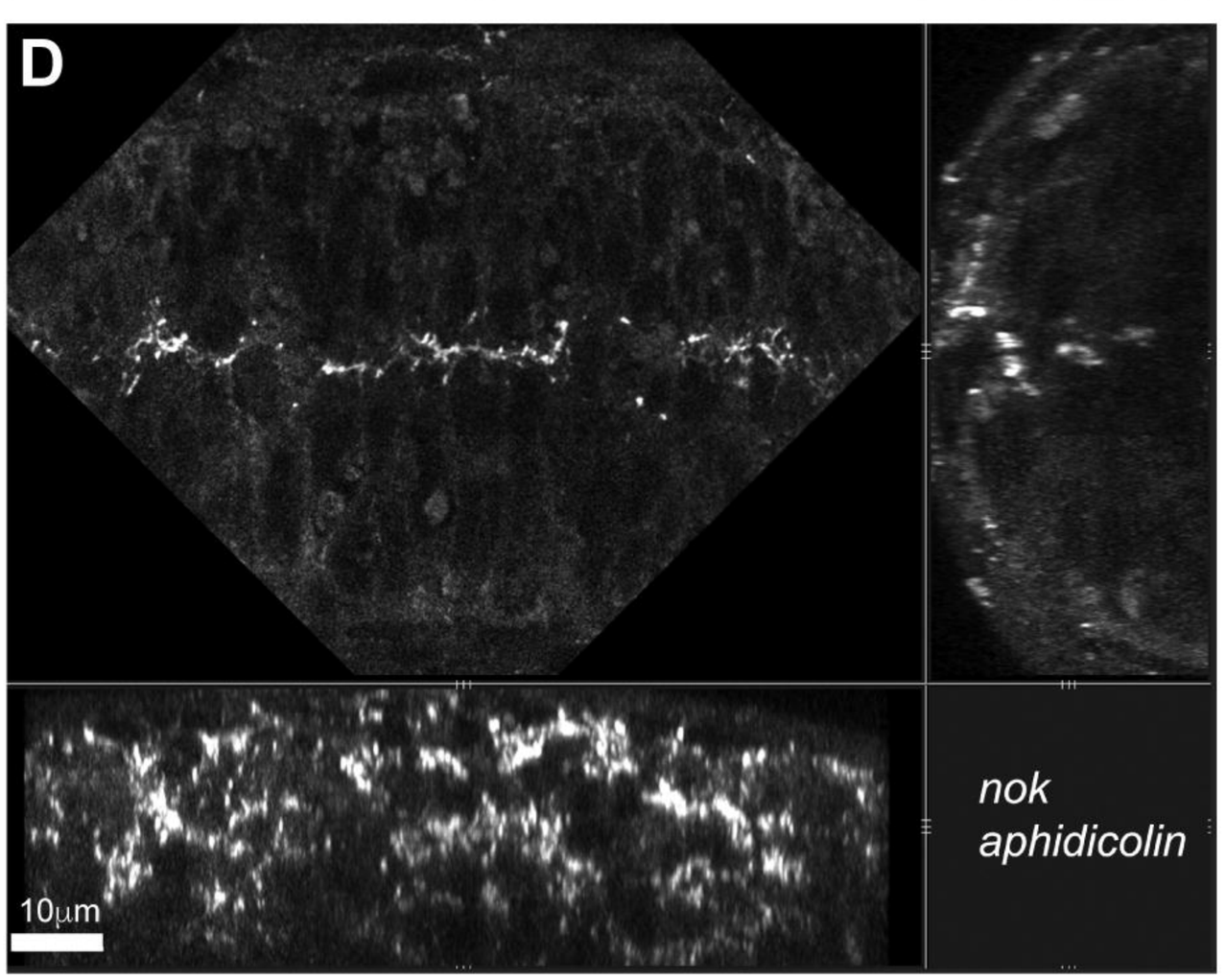
D
nok
aphidicolin
10μm

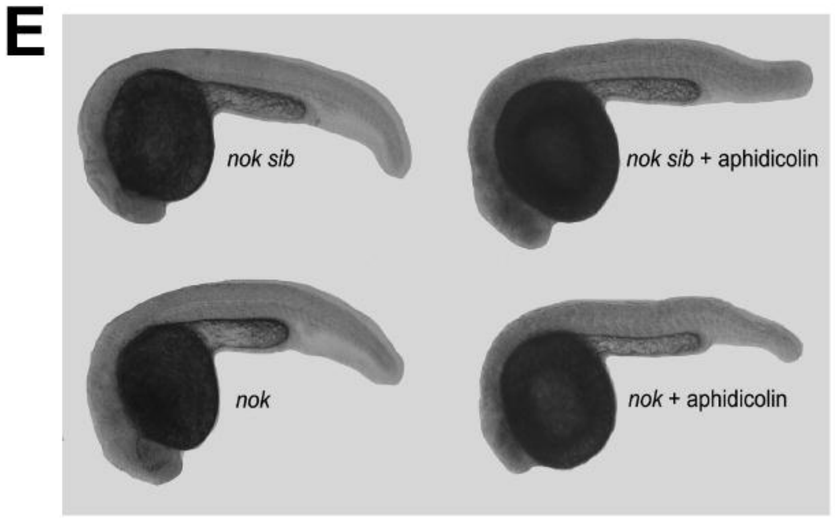
E
nok sib
nok sib + aphidicolin
nok
nok + aphidicolin

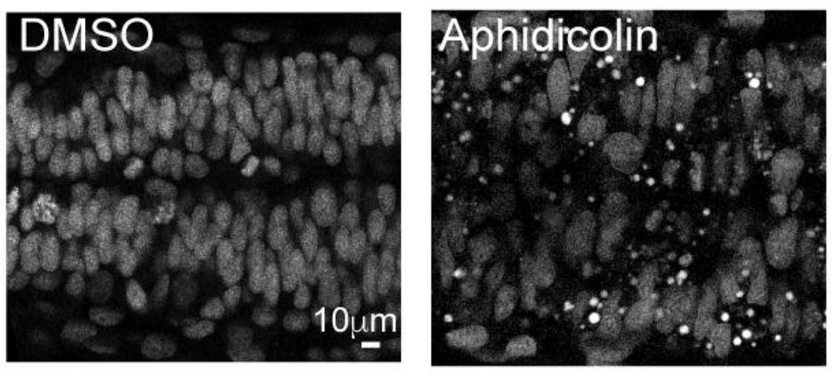
F
DMSO
Aphidicolin
10μm

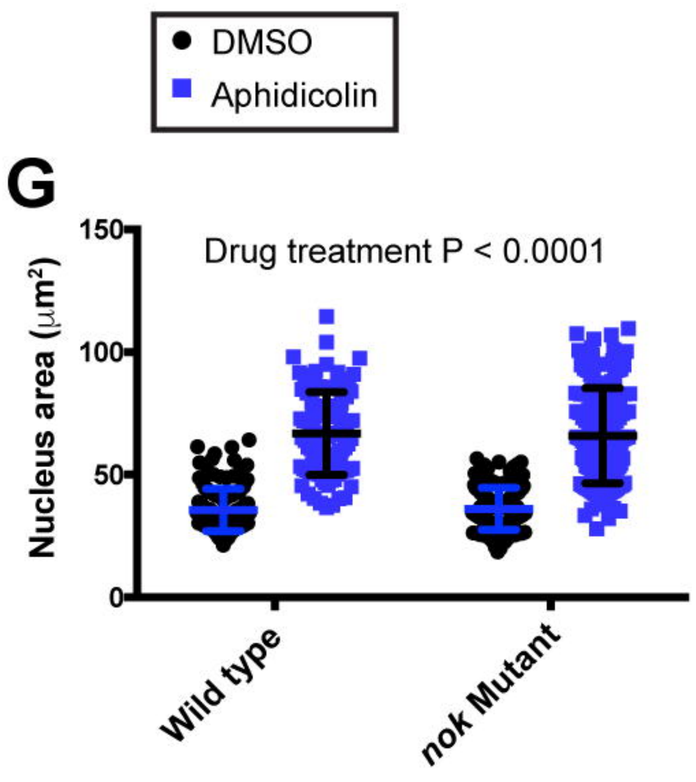
G
DMSO
Aphidicolin
Drug treatment P < 0.0001
Nucleus area (μm²)
150
100
50
0
Wild type
nok Mutant

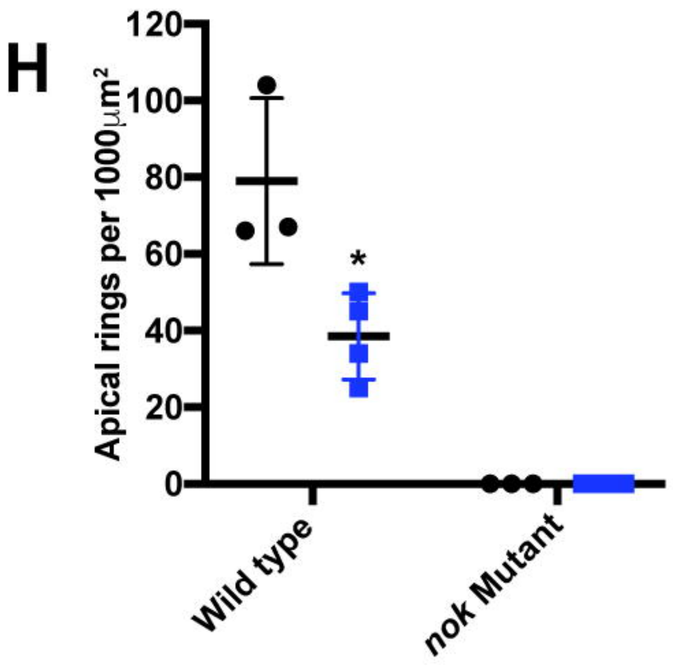
H
Apical rings per 1000μm²
120
100
80
60
40
20
0
*
Wild type
nok Mutant